



CERN-EP-2018-025

16 Feb 2018

Transverse momentum spectra and nuclear modification factors of charged particles in pp, p–Pb and Pb–Pb collisions at the LHC

ALICE Collaboration*

Abstract

We report the measured transverse momentum (p_T) spectra of primary charged particles from pp, p–Pb and Pb–Pb collisions at a center-of-mass energy $\sqrt{s_{NN}} = 5.02$ TeV in the kinematic range of $0.15 < p_T < 50$ GeV/ c and $|\eta| < 0.8$. A significant improvement of systematic uncertainties motivated the reanalysis of data in pp and Pb–Pb collisions at $\sqrt{s_{NN}} = 2.76$ TeV, as well as in p–Pb collisions at $\sqrt{s_{NN}} = 5.02$ TeV, which is also presented. Spectra from Pb–Pb collisions are presented in nine centrality intervals and are compared to a reference spectrum from pp collisions scaled by the number of binary nucleon-nucleon collisions. For central collisions, the p_T spectra are suppressed by more than a factor of 7 around 6–7 GeV/ c with a significant reduction in suppression towards higher momenta up to 30 GeV/ c . The nuclear modification factor R_{pPb} , constructed from the pp and p–Pb spectra measured at the same collision energy, is consistent with unity above 8 GeV/ c . While the spectra in both pp and Pb–Pb collisions are substantially harder at $\sqrt{s_{NN}} = 5.02$ TeV compared to 2.76 TeV, the nuclear modification factors show no significant collision energy dependence. The obtained results should provide further constraints on the parton energy loss calculations to determine the transport properties of the hot and dense QCD matter.

arXiv:1802.09145v2 [nucl-ex] 18 Jan 2019

© 2018 CERN for the benefit of the ALICE Collaboration.

Reproduction of this article or parts of it is allowed as specified in the CC-BY-4.0 license.

*See Appendix A for the list of collaboration members

1 Introduction

The properties of hot and dense deconfined QCD matter, the Quark-Gluon Plasma (QGP), which is formed in high-energy heavy-ion collisions, can be characterized by the measurement of high transverse momentum particles produced by hadronisation of hard scattered partons in the early stage of the collision. It is expected that these partons lose energy by interactions with the hot and dense QCD matter, which leads to jet quenching [1]. Manifested also as a suppression of high- p_T particles, jet quenching enables the extraction of the properties of the deconfined medium, in particular its transport coefficient \hat{q} [2].

The modification of high- p_T particle production is quantified with the nuclear modification factor R_{AA} , defined as the ratio of the charged-particle p_T spectrum in A–A collisions to that in pp collisions scaled by the average number of binary nucleon–nucleon collisions $\langle N_{\text{coll}} \rangle$ for a given centrality class of A–A collisions,

$$R_{AA} = \frac{dN^{AA}/dp_T}{\langle N_{\text{coll}} \rangle dN^{pp}/dp_T} = \frac{dN^{AA}/dp_T}{\langle T_{AA} \rangle d\sigma^{pp}/dp_T}, \quad (1)$$

where N^{AA} and N^{pp} are the charged-particle yields in A–A and pp collisions and σ^{pp} is the production cross section in pp collisions, respectively. The average nuclear overlap function, $\langle T_{AA} \rangle = \langle N_{\text{coll}} \rangle / \sigma_{\text{inel}}^{\text{NN}}$, which depends on the collision centrality, is determined from the Glauber model of the nuclear collision geometry [3], where $\sigma_{\text{inel}}^{\text{NN}}$ is the total inelastic nucleon-nucleon cross section. Over the years, a number of results on R_{AA} have been reported by experiments at the Relativistic Heavy-Ion Collider (RHIC) and at the Large Hadron Collider (LHC). At RHIC, the yields of charged hadrons [4, 5] or neutral pions [6] measured in the central Au–Au collisions at $\sqrt{s_{\text{NN}}} = 130$ and 200 GeV were found to be suppressed by a factor of about 5 in the p_T range of 5–25 GeV/ c , indicating for the first time strong medium effects on hadron production. The first R_{AA} measurements for charged particles at the LHC [7–10] have shown that in central Pb–Pb collisions at $\sqrt{s_{\text{NN}}} = 2.76$ TeV the yields are suppressed by a factor of up to 7 for $p_T = 6$ –7 GeV/ c . For larger p_T , the suppression decreases, but remains significant (a factor of about 2) in the range of 30–150 GeV/ c .

The first Pb–Pb collisions at $\sqrt{s_{\text{NN}}} = 5.02$ TeV were delivered by the LHC in 2015. Data in pp collisions at the same energy were also collected by the LHC experiments, allowing for a direct comparison of particle production in pp, p–Pb and Pb–Pb collisions. The first results on charged-particle R_{AA} at $\sqrt{s_{\text{NN}}} = 5.02$ TeV have recently become available from the CMS Collaboration [11], showing that in central Pb–Pb collisions charged-particle production is suppressed by a factor of 7–8 for $p_T = 6$ –9 GeV/ c . The suppression continues up to the highest p_T measured and approaches unity in the vicinity of $p_T = 200$ GeV/ c .

Measurements of p–Pb collisions at the LHC were performed to establish whether the initial state of the colliding nuclei plays a role in the observed suppression of high- p_T hadron production in Pb–Pb collisions. The $R_{p\text{Pb}}$ was found to be consistent with unity for p_T up to a few tens of GeV/ c , indicating that in this domain initial state effects do not influence particle production [12–15].

In this paper, we report the measurement of transverse momentum spectra of charged particles in pp and Pb–Pb collisions at $\sqrt{s_{\text{NN}}} = 5.02$ TeV. The resulting p_T spectra are used to determine the nuclear modification factors in Pb–Pb collisions at the highest energy currently accessible at the LHC. The p_T spectrum measured in pp collisions at the same collision energy as p–Pb is also used as the reference to calculate $R_{p\text{Pb}}$. These measurements allow us to compare the particle production in pp, p–Pb and Pb–Pb collisions at the same $\sqrt{s_{\text{NN}}}$, for the first time with ALICE at the LHC. In addition, we report a reanalysis of data collected in pp and Pb–Pb collisions at $\sqrt{s_{\text{NN}}} = 2.76$ TeV, and in p–Pb collisions at $\sqrt{s_{\text{NN}}} = 5.02$ TeV. The reanalysis is warranted by significant improvements in track selection and efficiency corrections, which benefit from the experience accumulated in the past years as well as better knowledge of the particle production at the LHC energies. This leads to significantly-reduced systematic

uncertainties by a factor of about 2 as compared to previously published results [8, 13, 16], which the current analysis supersedes. The increase in $\sqrt{s_{\text{NN}}}$ from 2.76 TeV to 5.02 TeV for Pb–Pb collisions leads to $\sim 20\%$ increase in the particle multiplicity [17] indicating that the larger medium density is reached at the higher collision energy. We characterize this medium by comparing the p_{T} spectra and nuclear modification factors measured at the two energies.

2 Experiment and data analysis

The data in Pb–Pb and pp collisions at $\sqrt{s_{\text{NN}}} = 2.76$ TeV and in p–Pb collisions at $\sqrt{s_{\text{NN}}} = 5.02$ TeV were collected with the ALICE apparatus [18] in 2010, 2011 and 2013, respectively. Details on the ALICE experimental conditions and the detector performance are given in [19]. The data in Pb–Pb and pp collisions at $\sqrt{s_{\text{NN}}} = 5.02$ TeV were recorded in 2015.

2.1 Trigger and event selection

The analysis is based on tracking information from the Inner Tracking System (ITS) [20] and the Time Projection Chamber (TPC) [21], both are located in the central barrel of the experiment and embedded in a solenoidal magnetic field of 0.5 T parallel to its axis.

The minimum-bias (MB) interaction trigger was based on signals from the forward scintillator arrays (V0A and V0C) and the two innermost layers of the ITS, the Silicon Pixel Detector (SPD), in coincidence with two beam bunches crossing in the ALICE interaction region. The pp collisions at $\sqrt{s} = 2.76$ TeV were selected requiring a signal in either one of the V0A or the V0C detectors or in the SPD. The Pb–Pb collisions at $\sqrt{s_{\text{NN}}} = 2.76$ TeV were selected based on different combinations of hits in the SPD and either V0A or V0C detector. The efficiency for hadronic interactions is approximately 100% in the 0–80% centrality range considered in this analysis, see details in [19]. For measurements of pp, p–Pb and Pb–Pb collisions at $\sqrt{s_{\text{NN}}} = 5.02$ TeV the trigger required a signal in both V0A and V0C detectors.

The offline event selection was optimized to reject beam-induced background in all collision systems. The background events were efficiently rejected by exploiting the timing signals in the two V0 detectors. In Pb–Pb collisions background was also rejected exploiting the correlation between the arrival times measured in each neutron Zero Degree Calorimeter (ZDC), positioned on both sides of the interaction point at 114.0 m for pp and Pb–Pb data at $\sqrt{s_{\text{NN}}} = 2.76$ TeV and at 112.5 m for the rest data sets. The contamination from electromagnetic interactions in Pb–Pb collisions was strongly suppressed using signals from the ZDCs (see [19] for details).

The primary event vertex is determined with tracks from the central barrel. For the analysis of pp collisions, if no vertex is found using tracks, the vertex reconstruction is performed using SPD tracklets; track segments reconstructed based on the information from the two innermost layers of the ITS. To ensure a uniform acceptance and reconstruction efficiency in the pseudorapidity region $|\eta| < 0.8$, only events with a reconstructed vertex within ± 10 cm from the center of the detector along the beam direction are used. It corresponds to around 2 standard deviations from the mean of the interaction region distribution (Gaussian shape) determined for all collisions systems and energies.

In Pb–Pb collisions, the centrality quantifies the fraction of the geometrical cross-section of the colliding nuclei, and it is related to their geometrical overlap region. It is determined using the sum of the amplitudes of the V0A and V0C signals [22]. The analysis is limited to the 0–80% most central events, to ensure that effects of trigger inefficiency and contamination by electromagnetic processes [23], as well as possible biases in the selection of more peripheral events [24], are negligible. The average quantities characterizing a centrality class, such as the mean number of participants $\langle N_{\text{part}} \rangle$, the mean number of binary collisions $\langle N_{\text{coll}} \rangle$ or the average nuclear overlap function $\langle T_{\text{AA}} \rangle$ were obtained [22] by fitting the experimental distributions with a Glauber Monte Carlo model [3], coupled to the model of particle production with $f \cdot N_{\text{part}} + (1 - f) \cdot N_{\text{coll}}$ particle sources, each source producing particles according to a Neg-

collision system	$\sqrt{s_{\text{NN}}} = 2.76 \text{ TeV}$	$\sqrt{s_{\text{NN}}} = 5.02 \text{ TeV}$
pp	52 M	109 M
p-Pb	-	107 M
Pb-Pb (0–80%)	13 M	20 M

Table 1: Number of events used in the analysis for various systems and energies. The analysis of Pb–Pb events was performed for the 0–80% centrality range.

ative Binomial Distribution (NBD). This approach is inspired by two-component models [25, 26], which decompose nucleus-nucleus collisions into soft and hard interactions, where the soft interactions produce particles with an average multiplicity proportional to N_{part} , and the probability for hard interactions to occur is proportional to N_{coll} . The fit parameter f represents the contribution of soft processes to the particle production and amounts to about 0.8 for the two energies. In this calculations, we used an inelastic nucleon–nucleon cross-section $\sigma_{\text{NN}} = (67.6 \pm 0.6) \text{ mb}$ for $\sqrt{s_{\text{NN}}} = 5.02 \text{ TeV}$ and $\sigma_{\text{NN}} = (61.8 \pm 0.9) \text{ mb}$ for $\sqrt{s_{\text{NN}}} = 2.76 \text{ TeV}$, obtained by interpolation [3] of the existing world data.

In p–Pb collisions, the average quantities $\langle N_{\text{part}} \rangle$, $\langle N_{\text{coll}} \rangle$ and $\langle T_{\text{pPb}} \rangle$ were determined [22] following the procedure described in [27], with the updated inelastic nucleon–nucleon cross-section $\sigma_{\text{NN}} = (67.6 \pm 0.6) \text{ mb}$ at $\sqrt{s_{\text{NN}}} = 5.02 \text{ TeV}$ and nuclear density function. In order to omit potential biases on the p_{T} spectra related to p–Pb collision centrality determination [27], only p–Pb events in the 0–100% centrality interval were used in the presented analysis.

The number of events satisfying the trigger and offline selection criteria for various collision systems and energies are listed in Table 1.

2.2 Track selection

Primary charged particles are measured in the kinematic range $|\eta| < 0.8$ and $0.15 < p_{\text{T}} < 50 \text{ GeV}/c$. A primary charged particle is defined [28] to be a charged particle with a mean proper lifetime τ larger than $1 \text{ cm}/c$ which is either produced directly in the interaction, or from decays of particles with τ smaller than $1 \text{ cm}/c$, excluding particles produced in interactions with the detector material. The track-selection criteria were identical for all data sets and were optimized for best track quality and minimal contamination from secondary particles. Each track is required to have:

- at least 2 hits in the ITS detector, of which at least one hit is in the two innermost (SPD) layers;
- the length L (in cm) of its projection curve calculated in the TPC readout plane, excluding the information from the pads at the sector boundaries ($\sim 3 \text{ cm}$ from the sector edges), larger than $A - B \cdot p_{\text{T}}^C$, with $A = 130 \text{ cm}$, $B = 1.0 \text{ cm} \cdot (\text{GeV}/c)^{-C}$, $C = -1.5$ and p_{T} in units of GeV/c ;
- the number of crossed TPC pad rows larger than $0.85 \cdot L$ (the height of pad rows varies from 7.5 mm to 15 mm [21]); a TPC readout pad row is considered crossed if there is a cluster in this row and in any of its neighboring 2 rows;
- the number of TPC clusters (one cluster per pad row) larger than $0.7 \cdot L$;
- the ratio of crossed TPC pad rows to the number of findable TPC clusters (maximum number of clusters which can be assigned to a track in the TPC fiducial volume, excluding the information from the pads at the sector boundaries) larger than 0.8;
- the fraction of TPC clusters shared with another track lower than 0.4;
- the fit quality for the ITS and TPC track points satisfying $\chi_{\text{ITS}}^2/N_{\text{hits}} < 36$ and $\chi_{\text{TPC}}^2/N_{\text{clusters}} < 4$, respectively;

- $\chi_{\text{TPC-ITS}}^2 < 36$, where $\chi_{\text{TPC-ITS}}^2$ is calculated comparing the track parameters of the helix fit from the combined ITS+TPC track reconstruction to that derived only from the TPC and constrained by the interaction point, see details in [8];
- the distance of closest approach to the primary vertex in the transverse plane $|\text{DCA}_{xy}| < A + B \cdot p_T^C$, with $A = 0.0182$ cm, $B = 0.035$ cm $\cdot (\text{GeV}/c)^{-C}$, $C = -1.0$ and p_T in units of GeV/c; and along the beam axis $|\text{DCA}_z| < 2$ cm.

2.3 Corrections

The data are presented as differential cross sections for inelastic (INEL) pp collisions

$$\frac{d^2\sigma}{d\eta dp_T} = \sigma_{\text{MB}}^{\text{pp}} \cdot \frac{1}{N_{\text{ev}}^{\text{MB}}} \frac{d^2N}{d\eta dp_T} \equiv \sigma_{\text{MB}}^{\text{pp}} \cdot \frac{N^{\text{rec}}(\Delta\eta, \Delta p_T) \cdot C(\Delta\eta, \Delta p_T)}{N_{\text{ev}}^{\text{rec}} \cdot \Delta\eta \Delta p_T} \cdot \varepsilon_{\text{VZ}}, \quad (2)$$

and transverse momentum spectra for non-single diffractive (NSD) p–Pb and centrality-selected INEL Pb–Pb collisions

$$\frac{1}{N_{\text{ev}}} \frac{d^2N}{d\eta dp_T} \equiv \frac{N^{\text{rec}}(\Delta\eta, \Delta p_T) \cdot C(\Delta\eta, \Delta p_T)}{N_{\text{ev}}^{\text{rec}} \cdot \Delta\eta \Delta p_T} \cdot \varepsilon_{\text{MB}} \cdot \varepsilon_{\text{VZ}}, \quad (3)$$

which are obtained by correcting the charged particle yields N^{rec} reconstructed in the $(\Delta\eta, \Delta p_T)$ intervals for all detector effects that either influence the event reconstruction, and thus are relevant only for the overall normalization (event-level corrections), or influence the track reconstruction and are relevant for both the spectral shape and normalization (track-level corrections). The ε_{MB} and ε_{VZ} denote the MB trigger and event vertex reconstruction efficiencies, and $C(\Delta\eta, \Delta p_T)$ are track-level correction factors. One should note that the ε_{VZ} is calculated for the triggered events. In general, both the ε_{MB} and ε_{VZ} are multiplicity dependent. Details of the correction procedure and variables are described in the following.

2.3.1 Event-level corrections

In Eq. 2 the minimum-bias cross section $\sigma_{\text{MB}}^{\text{pp}}$ in triggered pp collisions is determined by the van-der-Meer scans and depends on the trigger settings, it was measured to be 55.4 ± 1.0 mb at $\sqrt{s} = 2.76$ TeV [29] and 51.2 ± 1.2 mb at $\sqrt{s} = 5.02$ TeV [30], with the MB trigger OR (V0A or V0C or SPD) and AND (V0A and V0C), respectively. The differential charged-particle yields $d^2N/d\eta dp_T$ were calculated for the MB event class ($N_{\text{ev}}^{\text{MB}}$) by normalizing to the number of reconstructed events $N_{\text{ev}}^{\text{rec}}$, which have a reconstructed event vertex within ± 10 cm from of the center of the detector and correcting for the event vertex reconstruction efficiency ε_{VZ} .

For INEL pp collisions, the ε_{VZ} was estimated using the PYTHIA 8 (Monash 2013 tune) event generator [31, 32] and GEANT3 [33] detector response model. The resulting values $\varepsilon_{\text{VZ}} = 88.3\%$ (97.7%) at $\sqrt{s} = 2.76$ (5.02) TeV were used for corrections.

For NSD p–Pb collisions, the efficiency of the trigger (ε_{MB}) and event vertex reconstruction (ε_{VZ}), as in Eq. 3, were estimated using GEANT3 detector simulation with a combination of event generators as described in [12]. The obtained values $\varepsilon_{\text{MB}} = 99.2\%$ and $\varepsilon_{\text{VZ}} = 98.6\%$ were used for corrections.

For Pb–Pb collisions, the trigger and event vertex reconstruction is fully efficient for the centrality intervals considered in this work, as estimated using Monte Carlo simulations with GEANT3 and HIJING [34] as event generator.

2.3.2 Track-level corrections

The differential charged-particle yields $d^2N/d\eta dp_T$ (Eqs 2 and 3) are obtained from the reconstructed yields of tracks $N^{\text{rec}}(\Delta\eta, \Delta p_T)$ corrected using correction factors $C(\Delta\eta, \Delta p_T)$, which are products of acceptance, efficiency, purity and p_T resolution.

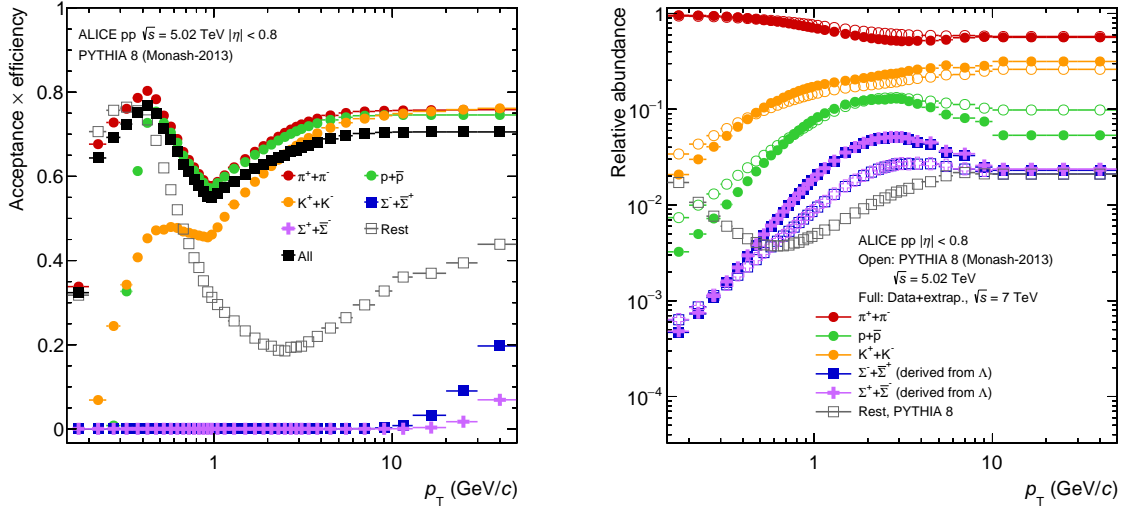


Figure 1: Left: Combined tracking efficiency and acceptance as a function of p_T for different particle species and the sum of all, obtained in Monte Carlo simulations of pp collisions at $\sqrt{s} = 5.02$ TeV with PYTHIA 8 (Monash 2013 tune). For $p_T > 1$ GeV/c parameterizations are shown. The relative systematic uncertainties on parameterizations are small ($< 0.2\%$) and are not shown. The statistical uncertainties for $p_T < 1$ GeV/c are smaller than the symbol size ($< 0.5\%$). Right: The relative particle abundances as a function of p_T in Monte Carlo (open symbols, for $\sqrt{s} = 5.02$ TeV) and in data (full symbols, for $\sqrt{s} = 7$ TeV) [35–37]. The data are extrapolated beyond the range of the measurements (see description in the text). The statistical and systematic uncertainties (combined $< 1.6\%$) are not shown.

The efficiency and purity of the primary charged particle reconstruction as well as acceptance correction for the pp, p–Pb and Pb–Pb data are calculated using Monte Carlo event generators with GEANT3 detector modeling combined with data-driven corrections, which are discussed in detail in the following sections.

Tracking efficiency The efficiency of the primary charged particle reconstruction is shown in Fig. 1 (left). While the low efficiency at low p_T is related to the strong track curvature caused by the magnetic field and to the energy loss in the detector material, the characteristic shape around p_T of 1 GeV/c is caused primarily by the track length requirement. Tracks in this momentum range are more likely to cross the TPC sector boundaries and are thus reconstructed with lower efficiencies. The asymptotic value reached at high p_T reflects the acceptance limitations (detector boundaries and active channels) of the measurement.

The tracking efficiency depends on particle species, as can be seen in Fig. 1 (left), and was calculated using a detector simulation with the PYTHIA 8 (Monash 2013 tune) event generator and the GEANT3 transport code. The efficiency is particularly species-dependent at low p_T (below 0.5 GeV/c) due to differences in ionization energy loss in the detector material, hadronic interaction cross-section or decay probability.

A particular case is that of charged hyperons, for which the reconstruction efficiency is very low and essentially negligible below 10 GeV/c, due to the fact that they decay before any significant interaction with the detector. For higher p_T , they reach the detector and can be observed with increasing efficiency. One should note that the reconstruction efficiency is different for the Σ^+ and Σ^- hyperons in the p_T range considered, because of their different lifetimes. The tracking efficiency for other primary charged particle species, including electrons, muons and Ξ and Ω hyperons (denoted as "Rest") is also shown.

In order to reduce statistical fluctuations at high p_T , we parameterized the efficiency above $p_T = 1$ GeV/c for each particle species. Each parameterization is a combination of the universal (independent of particle species) function $f(p_T) = a(1 - b \cdot e^{-cp_T})$ and the survival probability $P(p_T) = e^{-d \cdot m/p_T \cdot \tau}$ that a particle with the mass m and a mean proper lifetime τ survives a minimal distance d before decaying. The fitting parameters (a , b and c) are determined from the fit to the efficiency calculated as an average of efficiencies for stable particles. The calculations were performed for $d = 200$ cm, corresponding to the minimum track length in the ITS and the TPC required in the analysis.

The parametrized efficiencies shown in Fig. 1 (left) were used to determine data-driven correction factors in the efficiency reweighting procedure, which is discussed below.

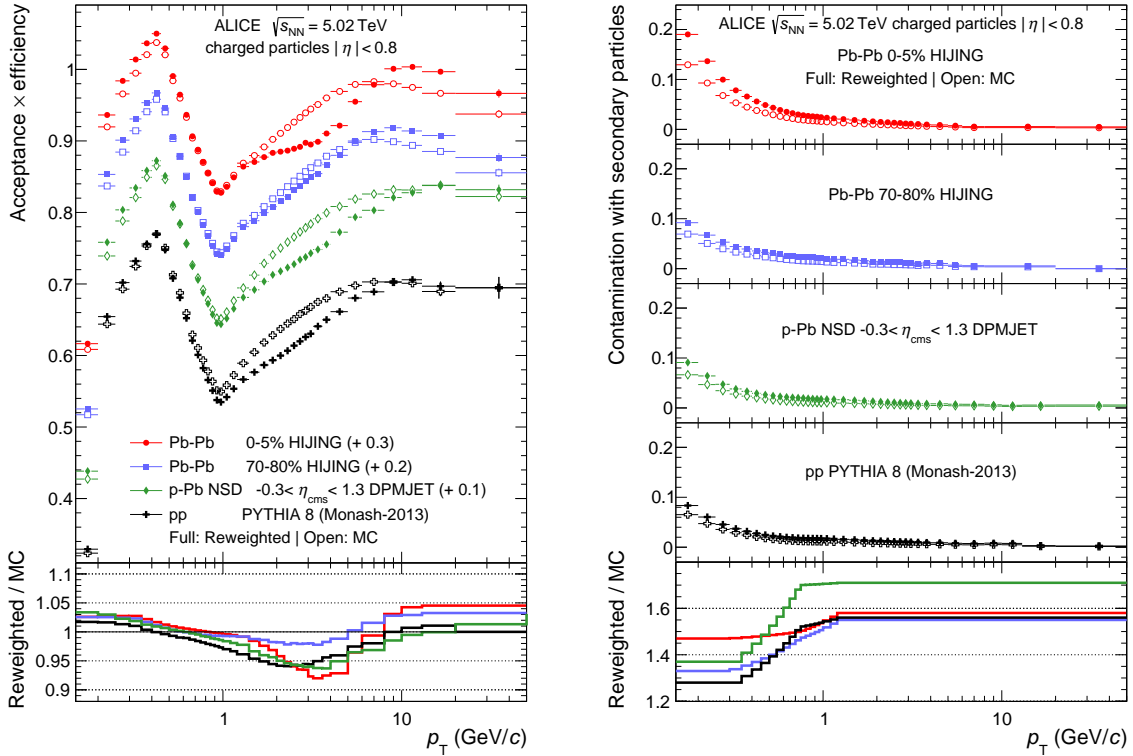


Figure 2: Left: Combined tracking efficiency and acceptance as a function of p_T for pp, p-Pb, central (0-5%) and peripheral (70-80%) Pb-Pb collisions determined using Monte Carlo simulations and a reweighting method (see text for details). For better visibility, the curves for p-Pb and Pb-Pb are offset by the indicated values. The effect of the reweighting on the efficiency corrections is shown in the bottom panel. The systematic uncertainties of the reweighting ($< 2.4\%$) are not shown. Right: Contamination from secondary particles estimated from Monte Carlo simulations and from the impact parameter fits in data (see text for details). The effect of the reweighting of secondary particles is shown in the bottom panel. The systematic uncertainties on the scaling factors ($< 20\%$) are not shown.

Reweighting with measured particle composition The experimental knowledge of the primary particle composition has significantly improved recently at the LHC [35–44], which allows for a precise determination of the tracking efficiency. For the first time, we determined the tracking efficiency by reweighting the primary particle composition based on data driven method.

In the right panel of Fig. 1, the relative particle abundances measured by ALICE in pp collisions at $\sqrt{s} = 7$ TeV are compared to those from Monte Carlo simulations with the PYTHIA 8 (Monash 2013 tune) event generator for $\sqrt{s} = 5.02$ TeV. Charged pions, kaons and protons were measured from p_T

= 0.15, 0.2, and 0.3 GeV/c to 20 GeV/c [35, 36], respectively. It is known that Monte Carlo event generators underestimate hyperon production substantially [38, 39]. In particular, the $\Sigma^+(1385)$ and $\Sigma^-(1385)$ hyperons and their antiparticles are underestimated by a factor of 2–3 in the recent PYTHIA 8 tunes. The p_T spectra of Σ^\pm hyperons have not been measured. Therefore, the p_T spectra of Σ^\pm are approximated using the measured spectrum of Λ hyperons [37] scaled by the ratio of Σ^\pm to Λ hyperons from the Monte Carlo generator.

Relative particle abundances measured in pp collisions at $\sqrt{s} = 7$ TeV are used to reweight the tracking efficiency determined for $\sqrt{s} = 2.76$ and 5.02 TeV collision energies, based on the experimental knowledge that their energy dependence is weak [37]. The relative abundance of other particle species containing electrons, muons and Ξ and Ω hyperons (denoted “Rest” in Fig. 1) is taken from simulations without further modification and has only a small influence on the final result ($< 1\%$). The measured p_T spectra of kaons, protons and Λ are extrapolated down to $p_T = 0.15$ GeV/c using a parameterization proposed by Bylinkin and Rostovtsev [45]. For high p_T , beyond the reach of the identified particle measurement, the relative abundances are assumed to be independent of p_T , as motivated by pQCD [46].

The reweighting of the efficiency has also been applied in the analysis of p–Pb and Pb–Pb data. The relative particle abundances obtained from Monte Carlo simulations with DPMJET (p–Pb) [47] and HIJING (Pb–Pb) event generators are reweighted using ALICE measurements of identified particle species (pions, kaons, protons and Λ hyperons) for p–Pb collisions at $\sqrt{s_{NN}} = 5$ TeV [36, 40] and Pb–Pb collisions at $\sqrt{s_{NN}} = 2.76$ TeV [41–44]. The relative particle abundances at low p_T are determined by extrapolating the measured p_T spectra of kaons, protons and Λ hyperons down to $p_T = 0.15$ GeV/c using a blast-wave parameterization [48]. As in the pp case, for p_T beyond the reach of these measurements, the relative abundances are assumed to be independent of p_T .

In the left panel of Fig. 2 the combined tracking efficiency and acceptance obtained from MC simulations (open symbols) and after reweighting (full symbols) is shown as a function of p_T for pp, p–Pb, and central (0–5%) and peripheral (70–80%) Pb–Pb collisions. The effect of the reweighting on the efficiency corrections is shown in the bottom panel. It amounts to a difference of about 7% at p_T around 3 GeV/c for the most central Pb–Pb collisions, and is lower in peripheral Pb–Pb collisions, p–Pb and pp collisions. When comparing central to peripheral Pb–Pb collisions, the importance of an increasing radial flow that shifts the heavy Σ^\pm baryons to larger momenta becomes apparent.

Purity The contribution from secondary particles, i.e. products of weak decays of kaons, Λ hyperons and muons, and particles arising from interactions in the detector material, was estimated using the transverse impact parameter d_{xy} distributions of particles in data and Monte Carlo simulations. Exploiting the differences, especially in the tails, of the d_{xy} distributions between primary and secondary particles, the measured distributions were fitted by a linear combination of d_{xy} distributions (templates) for primary and secondary particles obtained from the Monte Carlo simulations in different p_T bins (as described in more detail in [41]). The effect of this data-driven correction, shown in the bottom panel of Fig. 2 (right), depends on p_T and is different for pp, p–Pb and Pb–Pb collisions. The resulting contamination with secondary particles, i.e. the fraction of secondary particles in the sample of selected particles, ranges from 8.5% in pp to 20% in central Pb–Pb collisions at $p_T = 0.15$ GeV/c and decreases to around 1.0% for $p_T > 5$ GeV/c, as shown in the upper panel of Fig. 2 (right).

Transverse momentum resolution The transverse momentum of charged particles is reconstructed from the track curvature measured in the ITS and the TPC (see [19] for details). The modification of the spectra arising from the finite momentum resolution is estimated from the error obtained from the corresponding covariance matrix element of the Kalman fit. The relative p_T resolution, $\sigma(p_T)/p_T$, depends on momentum and is approximately 3–4% at $p_T = 0.15$ GeV/c, has a minimum of 1.0% at $p_T = 1.0$ GeV/c, and increases linearly for larger p_T , approaching 3–10% at 50 GeV/c, depending on collision energy, system or Pb–Pb centrality interval. The p_T resolution has been verified by studying the

Source of Uncertainty	pp		p-Pb	Pb-Pb	
	2.76 TeV	5.02 TeV	5.02 TeV	2.76 TeV	5.02 TeV
Event selection	0.9	0.5	0.1	1.5	0.14
Track selection	0.4–3.8	0.6–3.5	0.6–3.8	1.0–2.0	0.6–4.9
Secondary particles	0.5–5.1	0.0–2.8	0.0–2.1	0.0–4.0	0.0–4.5
Particle composition	0.1–1.6	0.2–2.4	0.4–2.2	0.0–2.0	0.2–2.0
Matching efficiency	1.0–4.0	0.0–1.1	0.3–3.2	0.2–2.0	0.2–1.2
Trigger and vertex selection	0.0–0.5	0.0–1.2	–	–	–
p_T resolution	0.0–3.0	0.0–1.4	0.0–3.0	0.0–2.7	0.0–1.0
Interaction rate	–	0.0	–	–	1.0
Material budget	0.1–0.9	0.1–0.9	0.1–0.9	0.1–0.9	0.1–0.9
Acceptance	–	–	0.0–0.2	–	–
Combined Uncertainty	3.5–6.2	1.3–4.3	1.7–5.1	1.9–5.2	1.0–7.5
Normalization	1.9	2.3	3.1	–	–
Centrality	–	–	–	0.1–3.6	0.1–3.5

Table 2: Contributions to the relative systematic uncertainty for p_T spectra in pp, p-Pb, and Pb-Pb collisions. The ranges correspond to the maximal variation within the considered p_T range of 0.15–50 GeV/c, as well as Pb-Pb centrality intervals. The p_T -dependent contributions are assumed to be independent and are summed in quadrature, resulting in the combined uncertainty. All values are in %.

widths of the invariant mass distributions of K_S^0 reconstructed from their decays to two charged pions.

To account for the finite p_T resolution, correction factors to the spectra were determined based on the Bayesian unfolding approach [49] implemented in the RooUnfold package [50]. This unfolding is based on the response matrix, $\mathbf{R}_{m,t}^{\text{det}}$, which relates the measured spectrum \mathbf{M}_m and the true spectrum \mathbf{T}_t , $\mathbf{M}_m = \mathbf{R}_{m,t}^{\text{det}} \cdot \mathbf{T}_t$, where m and t are indices indicating the bin number. The response matrix was generated for each data set and Pb-Pb collision centrality using GEANT3 detector simulations with different Monte-Carlo generators. For $p_T > 10$ GeV/c, another unfolding procedure similar to what was done in previous work [16] was also used.

The correction factors depend on the collision energy and system as well as on the collision centrality, due to the change of the spectral shape. For momenta below 10 GeV/c, the corrections are significant only in the first momentum bin $p_T = 0.15\text{--}0.2$ GeV/c, and reach 3%(2.5%) for pp(Pb-Pb) at $\sqrt{s_{\text{NN}}} = 2.76$ TeV, 3% for p-Pb at $\sqrt{s_{\text{NN}}} = 5.02$ TeV and around 1% for pp(Pb-Pb) at $\sqrt{s_{\text{NN}}} = 5.02$ TeV. At low p_T , these corrections are independent of Pb-Pb collision centrality. For $p_T > 10$ GeV/c, both unfolding methods yield almost identical correction factors. For $\sqrt{s_{\text{NN}}} = 5.02$ TeV, the correction factors reach 5%, 1.5% and 3% (4%) at $p_T = 50$ GeV/c for pp, p-Pb and 0-5%(70–80%) central Pb-Pb collisions, respectively. For $\sqrt{s_{\text{NN}}} = 2.76$ TeV, they amount to 4% for pp and 4% (8%) for 0-5%(70–80%) central Pb-Pb collisions at the highest p_T . The resulting p_T -dependent correction factors are applied (bin-by-bin) to the measured p_T spectra.

Trigger and vertex selection The event selection (trigger and vertex) introduces a small p_T -dependence in the correction on the p_T spectra in pp collisions. This is due to the fact that the low-multiplicity pp events, which are also characterized by a softer spectrum, are mostly rejected by the trigger and vertex selection criteria. The effect on the p_T spectra was calculated from simulations with the PYTHIA 8 (Monash 2013 tune) and the PYTHIA 6 (Perugia2011 tune) event generators and was estimated to be around 0.4–0.6% (2.2–2.6%) for $p_T < 1$ GeV/c at $\sqrt{s} = 2.76$ (5.02) TeV. The spectra are corrected by the average bias of these two generators, resulting in 0.5% (2.4%) corrections to the spectra.

Acceptance correction for the p-Pb data The two-in-one magnet design of the LHC imposes the same magnetic rigidity of the beams in the two rings. The configuration for p-Pb collisions with pro-

tons at 4 TeV energy colliding with $^{208}_{82}\text{Pb}$ ions at 82×4 TeV results in a shift in the rapidity of the nucleon–nucleon center-of-mass system by $\Delta y_{\text{NN}} = 0.465$ in the direction of the proton beam (negative z -direction). Therefore the detector coverage $|\eta_{\text{lab}}| < 0.8$ corresponds to roughly $-0.3 < \eta_{\text{cms}} < 1.3$. For massless or high p_{T} particles, $\eta_{\text{cms}} = \eta_{\text{lab}} + y_{\text{NN}}$ but the differential yield of non-massless particles at low p_{T} suffers from a distortion, which is estimated and corrected for based on the HIJING event generator weighted by the measured relative particle abundances [36, 40]. For $p_{\text{T}} = 0.5$ GeV/ c the correction is 2% for $-0.3 < \eta_{\text{cms}} < 1.3$.

2.4 Systematic uncertainty

The relative systematic uncertainties on the p_{T} spectra are summarized in Table 2.

- The effect of the selection of events based on the vertex position is studied by comparing the fully corrected p_{T} spectra obtained with alternative vertex selections corresponding to ± 5 and ± 20 cm.
- The systematic uncertainties related to the track selection criteria (listed above) were studied by varying the track quality cuts. In particular, we varied the upper limits of the track fit quality parameters in the ITS ($\chi^2_{\text{ITS}}/N_{\text{hits}}$) and the TPC ($\chi^2_{\text{TPC}}/N_{\text{clusters}}$) in the ranges of 25–49 and 3–5, respectively. The systematic uncertainties related to high- p_{T} fake tracks [8] were estimated by modifying the upper limits of the track matching criteria given by the $\chi^2_{\text{TPC-ITS}}$ in the range of 25–49. The resulting uncertainty dominates at high p_{T} for all collision systems.
- The systematic uncertainty on the secondary-particle contamination (Fig. 2, right) includes contributions from the template fits to the measured impact parameter distributions. We have varied the fit model using templates with two (primaries, secondaries) or three (primaries, secondaries from material, secondaries from weak decays of K^0_{s} and Λ) components, as well as the fit ranges. The maximum difference between the data and the 2 component-template fit is summed in quadrature with the difference between results obtained from the 2 and the 3 component-template fits and result is assigned as the systematic uncertainty on the contamination. This contribution dominates for the lowest p_{T} independently of the collision system.
- The systematic uncertainty on the primary particle composition consists of several contributions, including the extrapolation of the spectra to low p_{T} , the approximation of the relative particle abundances at high p_{T} , the efficiency parameterization at high p_{T} , the uncertainties of the measured particle spectra and the MC assumptions on the Σ^{\pm}/Λ spectra ratios. For the extrapolation to low p_{T} , we have studied different parameterizations (Bylinkin and Rostovtsev, modified Hagedorn [51], Blast-Wave) and fit ranges. We have varied the p_{T} thresholds for the approximation of the relative particle abundances as well as the efficiency parameterization at high p_{T} . The measured particle spectra were varied within systematic uncertainties (one particle species at a time), and the resulting differences to the nominal spectra were added in quadrature to the systematic uncertainties. We have also assigned an additional uncertainty related to the different spectral shape of Σ^{\pm} and Λ from the MC generators.
- To account for the imperfect description of the experimental setup in simulations, we compared the track matching between the TPC and the ITS information in data and Monte Carlo after scaling of the fraction of secondary particles obtained from the fits to the d_{xy} distributions. After rescaling the fraction of secondary particles, the agreement between data and Monte Carlo is within 4%. This value is assigned as an additional systematic uncertainty.
- The systematic uncertainty on the p_{T} resolution at low p_{T} (only first p_{T} bin) was estimated by changing Monte-Carlo generators in the unfolding procedure. The pp collisions were simulated with PYTHIA and PHOJET, p–Pb collisions with HIJING and DPMJET, and Pb–Pb collisions

with HIJING and AMPT [52]. The average correction factor of two generators was assigned as systematic uncertainty. At low p_T , we observe a weak dependence of correction factors on the considered Monte-Carlo generators. The resulting uncertainties amount to 3%(2.5%) for pp(Pb–Pb) collisions at $\sqrt{s_{NN}} = 2.76$ TeV, to 3% for p–Pb collisions at $\sqrt{s_{NN}} = 5.02$ TeV, and to 1% for pp and Pb–Pb collisions at $\sqrt{s_{NN}} = 5.02$ TeV. The systematic uncertainty on the p_T resolution at high p_T (> 10 GeV/c) was estimated using the azimuthal angle dependence of the $1/p_T$ spectra for positively and negatively charged particles. The relative shift of the spectra for oppositely charged particles along $1/p_T$ determines the size of uncertainty for a given angle. We used the RMS of the $1/p_T$ shift distribution for the full azimuth as additional smearing of the p_T resolution. We checked that these shifts are due to detector effects (such as $\mathbf{E} \times \mathbf{B}$ effect) and are not related to the physics of hadronic interaction in GEANT3. To take into account the decrease in the p_T resolution with increasing interaction rate, we have studied the systematic uncertainty for the pp and Pb–Pb data sets at $\sqrt{s_{NN}} = 5.02$ TeV, obtained from the difference of the spectra at high and low interaction rate. The uncertainty is negligible for pp collisions, and is about 1% for Pb–Pb collisions.

- For the correction due to the trigger and vertex selection, calculated as the average bias of two generators, half of the value is assigned as systematic uncertainty.
- The systematic uncertainty for the acceptance correction on the p–Pb data was estimated by varying the relative particle abundances within their measured uncertainties and by changing the fit function for the low- p_T extrapolation. The uncertainty is sizable only at low p_T where it reaches 0.2%.
- The material budget in the simulation was varied by $\pm 4.5\%$ [19], resulting in the systematic uncertainty in the range of 0.1–0.9%.
- The normalization uncertainty on the spectra in pp collisions was propagated from the cross section measurements.
- The systematic uncertainties related to centrality selection were estimated by a comparison of the p_T spectra when the limits of the centrality classes are shifted due to an uncertainty of $\pm 0.5\%$ in the fraction of the hadronic cross section used in the analysis and by a comparison of results obtained using the SPD detector to estimate centrality as opposed to the V0A and V0C.

For the evaluation of the total systematic uncertainty all contributions are considered to be uncorrelated and they are summed in quadrature. The improved reconstruction and track selection in the reanalysis of pp and Pb–Pb data at $\sqrt{s_{NN}} = 2.76$ TeV and p–Pb data at $\sqrt{s_{NN}} = 5.02$ TeV lead to significantly reduced systematic uncertainties by a factor of about 2 as compared to previously published results [8, 13, 16].

3 Results and discussion

3.1 Spectra

The fully corrected p_T spectra of primary charged particles measured in INEL pp and Pb–Pb collisions at $\sqrt{s_{NN}} = 2.76$ TeV and 5.02 TeV and in NSD p–Pb collisions at $\sqrt{s_{NN}} = 5.02$ are shown in Fig. 3. The Pb–Pb spectra are presented in nine centrality classes. For pp collisions, the p_T -differential cross sections are divided by the corresponding inelastic nucleon-nucleon cross section at $\sqrt{s} = 2.76$ (61.8 mb) and 5.02 TeV (67.6 mb) [3], respectively. The relative systematic uncertainties for the various datasets are shown in the bottom panels. Substantial improvements in track selection and efficiency corrections have been achieved. However the uncertainty on the pp data at $\sqrt{s_{NN}} = 2.76$ TeV is still larger than for the data at $\sqrt{s_{NN}} = 5.02$ TeV due to larger number of inactive channels in the SPD [19], which affects the track reconstruction and the determination of the secondary particle contribution.

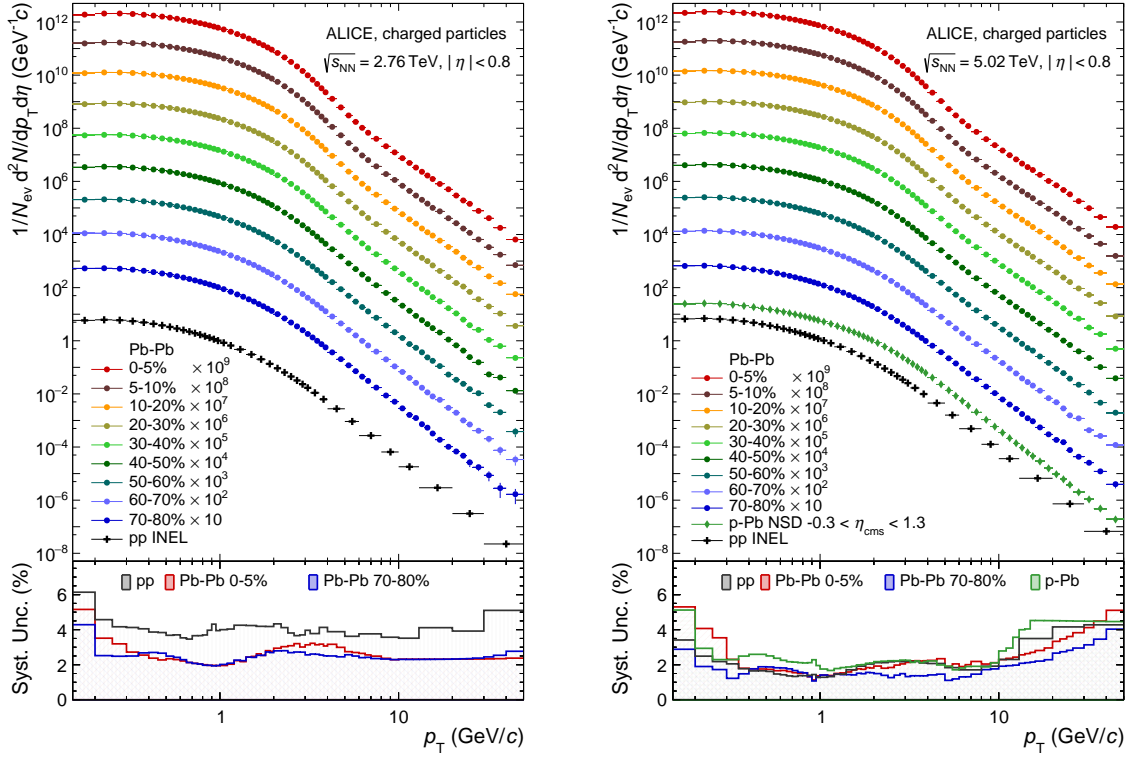


Figure 3: Transverse momentum distributions of primary charged particles in $|\eta| < 0.8$ in nine centrality intervals in Pb–Pb collisions at $\sqrt{s_{\text{NN}}} = 2.76$ (left) and 5.02 TeV (right) (scale factors as indicated are used for better visibility). The data for pp collisions, obtained scaling the cross section by $\sigma_{\text{inel}}^{\text{NN}}$, and NSD p–Pb at $\sqrt{s_{\text{NN}}} = 5.02$ TeV are also shown. The relative systematic uncertainties are shown in the lower panels for various datasets; these do not contain the normalization uncertainty.

In Pb–Pb collisions the shape of the p_{T} spectrum varies strongly with collision centrality. For peripheral collisions, the spectral shape is similar to that measured in pp collisions as well as to the spectrum in p–Pb collisions. With increasing collision centrality, a marked depletion of the Pb–Pb spectra develops for $p_{\text{T}} > 5$ GeV/c. These measurements supersede our previous results [8, 13, 16], which allows for a better discrimination between jet quenching scenarios.

Figure 4 compares the measured p_{T} spectra in pp collisions with results from PYTHIA 8 (Monash-2013 tune), including colour reconnection, and EPOS LHC [53], which incorporates collective (flow-like) effects. These event generators show a similar description of the p_{T} spectra at both energies. They reproduce the spectral shape within 20%.

Figure 5 shows the ratios of p_{T} spectra measured at $\sqrt{s_{\text{NN}}} = 5.02$ and $\sqrt{s_{\text{NN}}} = 2.76$ TeV in Pb–Pb and pp collisions. The ratios for Pb–Pb collisions are determined in nine centrality classes ranging from 0–5% (top-left) to the 70–80% (bottom-right). As indicated by the ratios, the p_{T} spectra measured at higher collision energy are significantly harder for both Pb–Pb and pp collision systems. One can see that there is a similar energy dependence of the ratio for peripheral (70–80%) Pb–Pb and in pp collisions, while towards central Pb–Pb collisions a gradual reduction of the ratio is apparent.

3.2 Nuclear modification factors

In order to quantify in-medium modification of charged-particle transverse momentum spectrum, the nuclear modification factors are determined. Figure 6 shows the R_{AA} for Pb–Pb collisions measured at

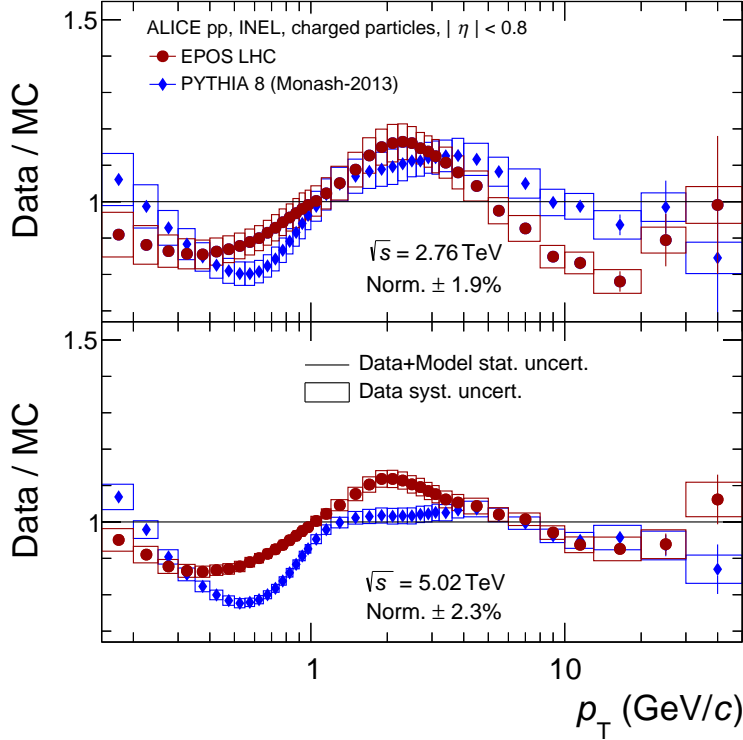


Figure 4: Comparison of the charged-particle transverse momentum spectra measured in pp collisions to PYTHIA 8 (Monash-2013 tune) [31, 32] and EPOS [53] model calculations at $\sqrt{s} = 2.76$ (top) and 5.02 TeV (bottom). The statistical uncertainties of the data and model calculations are added in quadrature. The boxes represent systematic uncertainties of the data.

$\sqrt{s_{\text{NN}}} = 2.76$ and 5.02 TeV. The nuclear modification factor has a strong centrality dependence, and is very similar in magnitude for the two collision energies.

Given that the p_T spectra are harder at the higher $\sqrt{s_{\text{NN}}}$ (see Fig. 5) and that the medium density increases with $\sqrt{s_{\text{NN}}}$ by $\sim 20\%$ [17], this similarity of the R_{AA} may indicate a larger parton energy loss in the hotter/denser and longer-lived deconfined medium produced at the higher center-of-mass energy. Assuming that the initial parton p_T spectrum, parton distribution and fragmentation functions are not significantly modified by the energy increase, and that the parton energy loss in expanding medium is sublinear to the medium density increase, we would expect larger energy loss at $\sqrt{s_{\text{NN}}} = 5.02$ TeV than at $\sqrt{s_{\text{NN}}} = 2.76$ TeV, but no more than 20%.

In 0–5% central collisions the yield is suppressed by a factor of about 8 ($R_{\text{AA}} \approx 0.13$) at $p_T = 6\text{--}7$ GeV/c. Above $p_T = 7$ GeV/c, there is a significant rise of the nuclear modification factor, which reaches a value of about 0.4 for our highest p_T bin, 30–50 GeV/c. In peripheral collisions (70–80%), the suppression is 30% for intermediate momenta and approaches unity for the highest p_T bin. The normalization uncertainties for R_{AA} originate from the pp measurement and centrality determination and were added in quadrature.

Figure 7 (left) shows the R_{pPb} factor compared to R_{AA} measured in the 0–5% and 70–80% centrality classes for Pb–Pb collisions at $\sqrt{s_{\text{NN}}} = 5.02$. The R_{pPb} factor exhibits a maximum for the intermediate p_T range, $2 < p_T < 6$ GeV/c, a feature generically called the Cronin effect [54]. A study on its dependence on the particle species [40] suggested that protons are responsible for the observed maximum. The maximum occurs at values of p_T (3–5 GeV/c) larger than the maximum of R_{AA} seen in the p_T range

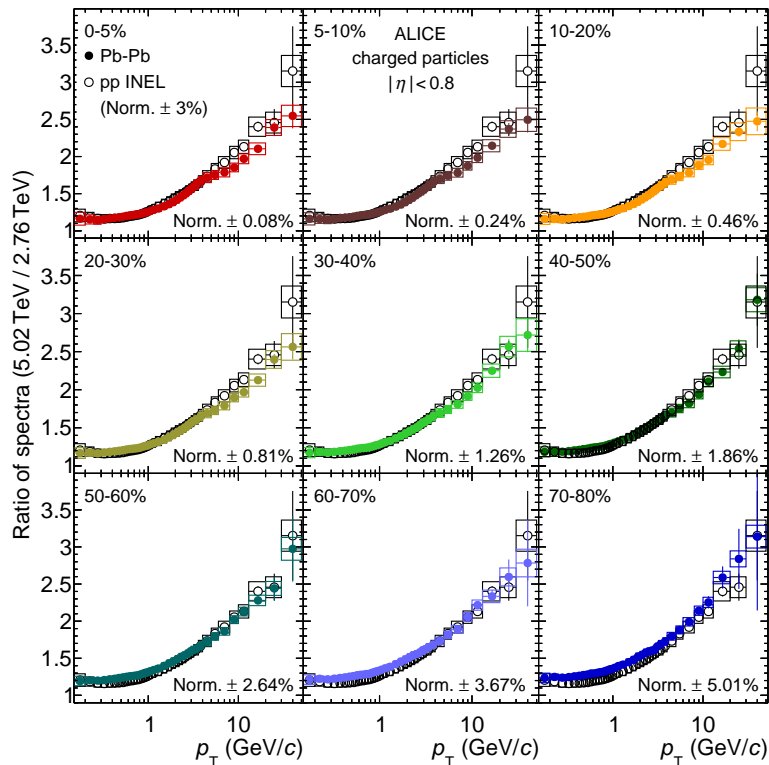


Figure 5: Ratio of transverse momentum spectra at $\sqrt{s_{\text{NN}}} = 5.02$ and $\sqrt{s_{\text{NN}}} = 2.76$ TeV for Pb–Pb collisions, for nine centrality classes, and in pp collisions (repeated in each panel). The relative normalization uncertainties due to the centrality determination are indicated for each centrality class. For the pp spectrum, the relative normalization uncertainty is $\pm 3\%$.

1.5–3 GeV/c. The R_{pPb} factor is consistent with unity for $p_{\text{T}} \gtrsim 8$ GeV/c, demonstrating that the strong suppression observed in central Pb–Pb collisions is not related to initial state effects but rather to the formation of hot and dense QCD matter. The ALICE results for R_{AA} and R_{pPb} measured at $\sqrt{s_{\text{NN}}} = 5.02$ TeV are compared to measurements by CMS [14] in Fig. 7 (right). Agreement within 1.5σ is observed for both R_{AA} and R_{pPb} taking into account the current uncertainties.

3.3 Comparison with theoretical models

In Fig. 8 the measured R_{AA} for 0-5% central collisions at $\sqrt{s_{\text{NN}}} = 5.02$ TeV is compared to model predictions. All presented models are based on the pQCD factorization, where the entire effect of energy loss is encoded in the medium-modified parton fragmentation function. All models include radiative energy loss based on different approaches. The model by Djordjevic et al. [57, 58] and CUJET 3.0 [60, 61] include in addition collisional energy loss. The energy loss is calculated in dynamically expanding medium in all models except that of Vitev et al. [55, 56], in which the medium is composed of static scattering centers. In the following, the models are discussed in more detail.

The calculations by Vitev et al. are based on the SCET_G model [55, 56], which uses an extended soft-collinear effective theory to describe inclusive particle production and suppression in the heavy-ion environment. This theoretical framework provides an analytic connection between generalized DGLAP evolution equations for the fragmentation functions in dense strongly-interacting matter and parton energy loss for hard processes. The calculations employ the pQCD-based hard cross section and QGP medium evolved parton-to-hadron fragmentation functions, combined with initial-state cold nuclear mat-

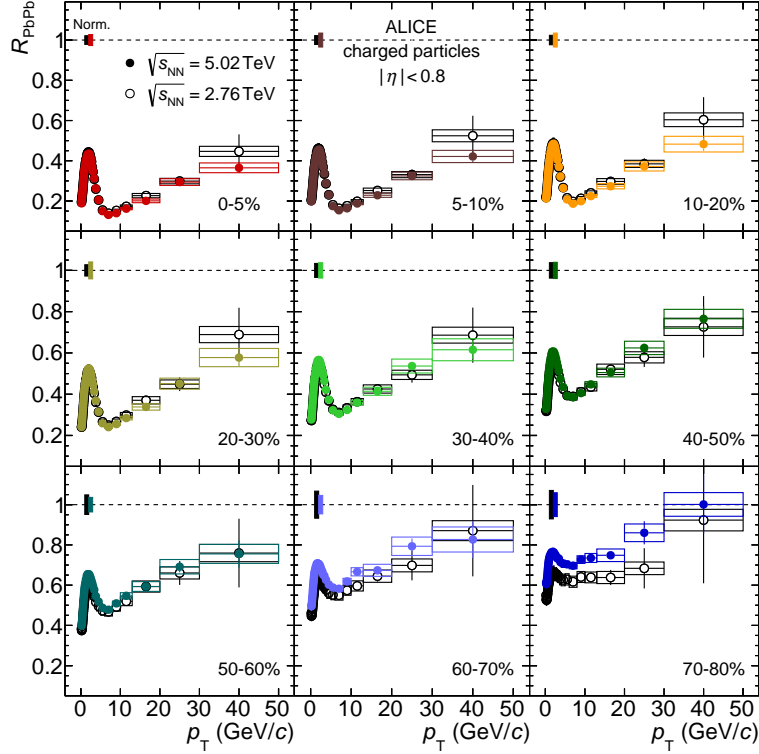


Figure 6: The transverse momentum dependence of the nuclear modification factor measured in Pb–Pb collisions, for nine centrality classes. The new data at $\sqrt{s_{\text{NN}}} = 5.02$ (full symbols) are compared to the reanalyzed data at $\sqrt{s_{\text{NN}}} = 2.76$ TeV (open symbols). The normalization uncertainties are shown as boxes around unity.

ter (CNM) effects, which include dynamical nuclear shadowing, the Cronin effect and initial-state parton energy loss (see [56] and references therein for details). The two upper and lower curves represent calculations for the nuclear modification factor with variations of the coupling strength $g = 1.9 \pm 0.1$ between the jet and the medium, which is a free parameter in the calculations. Djordjevic et al. [57, 58] use a dynamical energy loss formalism based on pQCD calculations in a finite size dynamical QCD medium. While the initial p_T spectrum is the same as that used in the SCET_G model, the dynamical description of the medium provides a consistent treatment of both radiative and collisional energy loss, including a finite magnetic screening mass, which modifies the gluon self energy and therefore changes the energy loss, as well as a running coupling constant for the strongly-interacting medium. The two curves correspond to different electric-to-magnetic screening mass ratios in the range $0.4 < \mu_M/\mu_E < 0.6$. The model of Bianchi et al. [59] uses the pQCD factorization scheme with a pQCD-based radiative energy loss in a hydrodynamically expanding medium. In this framework, high p_T hadrons arise from fragmentation of hard partons, which lose energy prior to hadronization via interactions with the medium. The amount of energy loss is regulated by the medium transport coefficient \hat{q} , which varies with the temperature-dependent entropy density of the medium as well as with the energy scale of jets propagating in the medium. The CUJET 3.0 model [60, 61] is an extension of the perturbative-QCD-based CUJET 2.0 model, with the two complementary non-perturbative features of the QCD cross-over phase transition: the suppression of quark and gluon degrees of freedom and the emergence of chromomagnetic monopoles. The calculations were performed varying the value of the QCD running coupling α_c from 0.95 to 1.33 for $Q < T_C$, and the ratio of electric to magnetic screening scales $c_m = g_s \mu_E/\mu_M$ ($c_m = 0, 0.3, 0.4$), where g_s is the strong coupling constant. The value of α_c was fixed for each c_m value by fitting a single reference datum, $R_{AA}(p_T = 12 \text{ GeV}/c) \approx 0.3$, for charged hadrons in 20–30% central

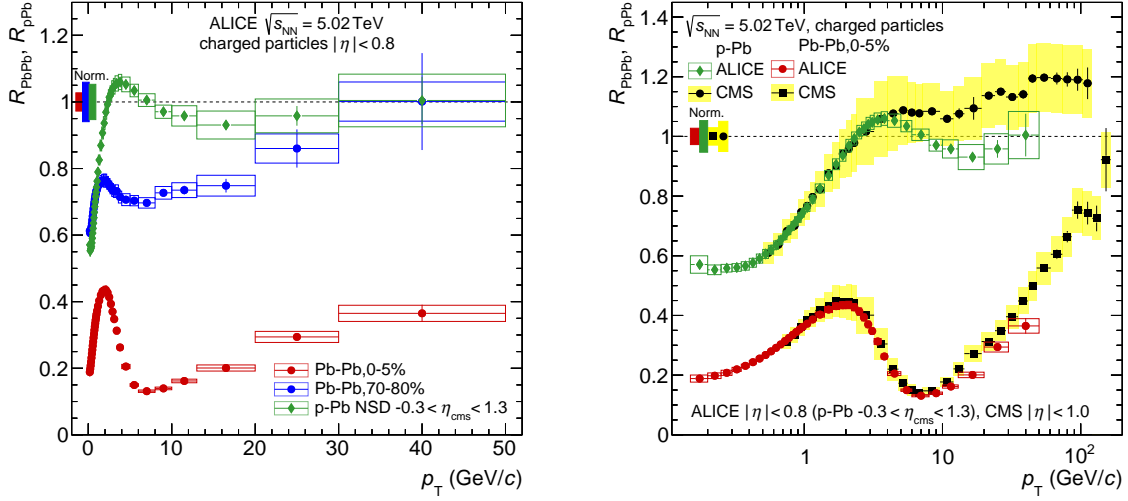


Figure 7: Left: Nuclear modification factors measured by ALICE in central (0–5%) and peripheral (70–80%) Pb–Pb collisions and in p–Pb collisions at $\sqrt{s_{NN}} = 5.02$ TeV. Right: A comparison of the nuclear modification factors for central (0–5%) Pb–Pb and p–Pb collisions measured by ALICE and CMS [11, 14]. In both figures, the p_T -dependent systematic uncertainties are shown as boxes around data points. The normalization uncertainties are shown as boxes around unity.

Pb–Pb collisions at the LHC. The calculations by Andrés et al. [62] use the jet quenching formalism of quenching weights. This approach consists of fitting a K factor, defined as $K \equiv \hat{q}/2\varepsilon^{3/4}$, that quantifies departure of this parameter from the perturbative estimate, $\hat{q}_{ideal} \sim 2\varepsilon^{3/4}$ [63], where the local energy density ε is taken from a hydrodynamical model of the medium. The K factor is the only free parameter in the fit of nuclear modification factors. Without including new data at $\sqrt{s_{NN}} = 5.02$ TeV in the fit procedure, they predict a $\sim 15\%$ larger suppression at $\sqrt{s_{NN}} = 5.02$ TeV as compared to $\sqrt{s_{NN}} = 2.76$ TeV, assuming the same value of K as the one obtained from the fit to the data at the lower energy.

All models presented here describe the main features of the data. The models by Vitev et al., Djordjevic et al. and CUJET 3.0 give quantitatively good description of the data. The model by Bianchi et al. is consistent with data within 1.5σ while that by Andrés et al. underestimates the data at high p_T . However, one should note that this comparison is made between unbinned theory calculations and binned data in relatively large p_T bins, which might introduce additional uncertainty.

4 Summary

In summary, we measured the primary charged particle p_T spectra in pp and Pb–Pb collisions at $\sqrt{s_{NN}} = 5.02$ TeV. We also reanalyzed the data collected in pp and Pb–Pb collisions at $\sqrt{s_{NN}} = 2.76$ TeV as well as in p–Pb collisions at $\sqrt{s_{NN}} = 5.02$ TeV with the revised techniques. Thanks to an improved reconstruction, track selection and data-driven efficiency correction procedure we were able to reduce the systematic uncertainties by a factor of ~ 2 as compared to previously published ALICE results. The measured spectra were used to determine the nuclear modification factors R_{pPb} and R_{AA} . The nuclear modification factor in p–Pb collisions is consistent with unity at high p_T , showing that the strong suppression observed in Pb–Pb is not due to CNM effects but rather due to final state partonic energy loss in the hot and dense QGP created in Pb–Pb collisions. This suppression is weak in peripheral collisions and increases with centrality reaching a value of $R_{AA} = 0.13$ at $p_T = 6$ – 7 GeV, indicating an increasing parton energy loss with centrality. This suppression is found to be similar at $\sqrt{s_{NN}} = 2.76$ and 5.02 TeV, despite the much harder p_T spectrum at the top energy, which may indicate a stronger parton energy loss

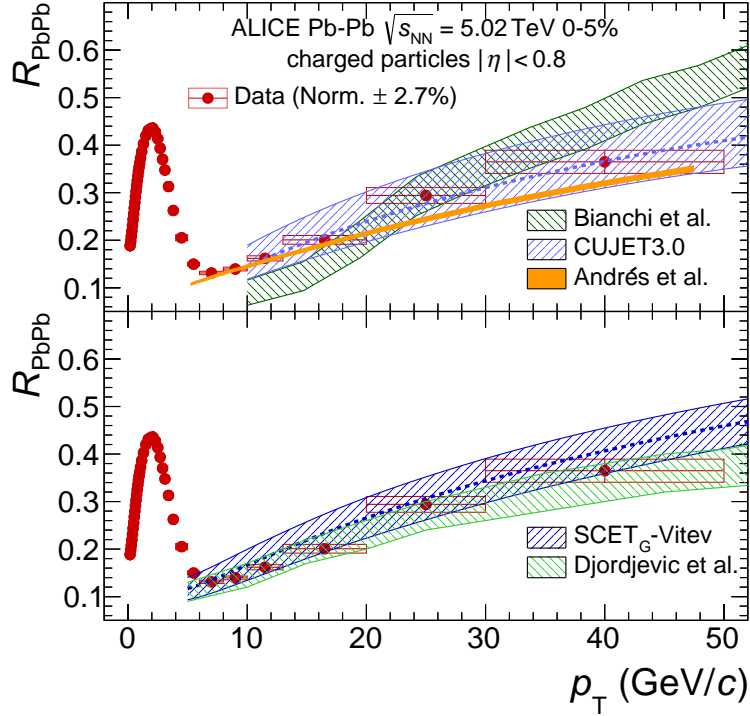


Figure 8: The charged-particle nuclear modification factor measured in the 0–5% most central Pb–Pb collisions at $\sqrt{s_{\text{NN}}} = 5.02$ TeV in comparison to model predictions [55–58] (lower panel) and [59–62] (upper panel). The red boxes around data points represent p_{T} dependent systematic uncertainties. The normalization uncertainty of the data ($\pm 2.7\%$) is not part of the uncertainties of the plotted data points.

and a larger energy density of the medium at the higher energy. All models presented here describe the main features of the data with Vitev et al., Djordjevic et al. and CUJET 3.0 being compatible with data within uncertainties. However, further precision in the theoretical calculations is needed to extract the transport properties of the hot and dense deconfined QCD matter.

Acknowledgements

The ALICE Collaboration would like to thank all its engineers and technicians for their invaluable contributions to the construction of the experiment and the CERN accelerator teams for the outstanding performance of the LHC complex. The ALICE Collaboration gratefully acknowledges the resources and support provided by all Grid centres and the Worldwide LHC Computing Grid (WLCG) collaboration. The ALICE Collaboration acknowledges the following funding agencies for their support in building and running the ALICE detector: A. I. Alikhanyan National Science Laboratory (Yerevan Physics Institute) Foundation (ANSL), State Committee of Science and World Federation of Scientists (WFS), Armenia; Austrian Academy of Sciences and Nationalstiftung für Forschung, Technologie und Entwicklung, Austria; Ministry of Communications and High Technologies, National Nuclear Research Center, Azerbaijan; Conselho Nacional de Desenvolvimento Científico e Tecnológico (CNPq), Universidade Federal do Rio Grande do Sul (UFRGS), Financiadora de Estudos e Projetos (Finep) and Fundação de Amparo à Pesquisa do Estado de São Paulo (FAPESP), Brazil; Ministry of Science & Technology of China (MSTC), National Natural Science Foundation of China (NSFC) and Ministry of Education of China (MOEC), China; Ministry of Science, Education and Sport and Croatian Science Foundation, Croatia; Ministry of Education, Youth and Sports of the Czech Republic, Czech Republic; The Danish Council

for Independent Research — Natural Sciences, the Carlsberg Foundation and Danish National Research Foundation (DNRF), Denmark; Helsinki Institute of Physics (HIP), Finland; Commissariat à l’Energie Atomique (CEA) and Institut National de Physique Nucléaire et de Physique des Particules (IN2P3) and Centre National de la Recherche Scientifique (CNRS), France; Bundesministerium für Bildung, Wissenschaft, Forschung und Technologie (BMBF) and GSI Helmholtzzentrum für Schwerionenforschung GmbH, Germany; General Secretariat for Research and Technology, Ministry of Education, Research and Religions, Greece; National Research, Development and Innovation Office, Hungary; Department of Atomic Energy Government of India (DAE), Department of Science and Technology, Government of India (DST), University Grants Commission, Government of India (UGC) and Council of Scientific and Industrial Research (CSIR), India; Indonesian Institute of Science, Indonesia; Centro Fermi - Museo Storico della Fisica e Centro Studi e Ricerche Enrico Fermi and Istituto Nazionale di Fisica Nucleare (INFN), Italy; Institute for Innovative Science and Technology, Nagasaki Institute of Applied Science (IIST), Japan Society for the Promotion of Science (JSPS) KAKENHI and Japanese Ministry of Education, Culture, Sports, Science and Technology (MEXT), Japan; Consejo Nacional de Ciencia (CONACYT) y Tecnología, through Fondo de Cooperación Internacional en Ciencia y Tecnología (FONCICYT) and Dirección General de Asuntos del Personal Académico (DGAPA), Mexico; Nederlandse Organisatie voor Wetenschappelijk Onderzoek (NWO), Netherlands; The Research Council of Norway, Norway; Commission on Science and Technology for Sustainable Development in the South (COMSATS), Pakistan; Pontificia Universidad Católica del Perú, Peru; Ministry of Science and Higher Education and National Science Centre, Poland; Korea Institute of Science and Technology Information and National Research Foundation of Korea (NRF), Republic of Korea; Ministry of Education and Scientific Research, Institute of Atomic Physics and Romanian National Agency for Science, Technology and Innovation, Romania; Joint Institute for Nuclear Research (JINR), Ministry of Education and Science of the Russian Federation and National Research Centre Kurchatov Institute, Russia; Ministry of Education, Science, Research and Sport of the Slovak Republic, Slovakia; National Research Foundation of South Africa, South Africa; Centro de Aplicaciones Tecnológicas y Desarrollo Nuclear (CEADEN), Cubaenergía, Cuba and Centro de Investigaciones Energéticas, Medioambientales y Tecnológicas (CIEMAT), Spain; Swedish Research Council (VR) and Knut & Alice Wallenberg Foundation (KAW), Sweden; European Organization for Nuclear Research, Switzerland; National Science and Technology Development Agency (NSDTA), Suranaree University of Technology (SUT) and Office of the Higher Education Commission under NRU project of Thailand, Thailand; Turkish Atomic Energy Agency (TAEK), Turkey; National Academy of Sciences of Ukraine, Ukraine; Science and Technology Facilities Council (STFC), United Kingdom; National Science Foundation of the United States of America (NSF) and United States Department of Energy, Office of Nuclear Physics (DOE NP), United States of America.

References

- [1] J. Bjorken, “Energy loss of energetic Partons in quark - gluon plasma: possible extinction of high p_T jets in hadron - hadron collisions,” Tech. Rep. FERMILAB-PUB-82-059-T, Fermilab, 1982. <http://lss.fnal.gov/archive/preprint/fermilab-pub-82-059-t.shtml>.
- [2] **JET** Collaboration, K. M. Burke *et al.*, “Extracting the jet transport coefficient from jet quenching in high-energy heavy-ion collisions,” *Phys. Rev.* **C90** (2014) 014909, arXiv:1312.5003 [nucl-th].
- [3] C. Loizides, J. Kamin, and D. d’Enterria, “Improved Monte Carlo Glauber predictions at present and future nuclear colliders,” *Phys. Rev.* **C97** (2018) 054910, arXiv:1710.07098 [nucl-ex].
- [4] **PHENIX** Collaboration, K. Adcox *et al.*, “Suppression of hadrons with large transverse momentum in central Au+Au collisions at $\sqrt{s_{NN}} = 130$ GeV,” *Phys. Rev. Lett.* **88** (2002) 022301, arXiv:nucl-ex/0109003 [nucl-ex].

- [5] **STAR** Collaboration, C. Adler *et al.*, “Centrality dependence of high p_T hadron suppression in Au+Au collisions at $\sqrt{s_{NN}} = 130$ GeV,” *Phys. Rev. Lett.* **89** (2002) 202301, arXiv:nuc1-ex/0206011 [nucl-ex].
- [6] **PHENIX** Collaboration, A. Adare *et al.*, “Suppression Pattern of Neutral Pions at High Transverse Momentum in Au+Au Collisions at $\sqrt{s_{NN}} = 200$ GeV and Constraints on Medium Transport Coefficients,” *Phys. Rev. Lett.* **101** (2008) 232301, arXiv:0801.4020 [nucl-ex].
- [7] **ALICE** Collaboration, K. Aamodt *et al.*, “Suppression of charged Particle production at large transverse momentum in central Pb–Pb collisions at $\sqrt{s_{NN}} = 2.76$ TeV,” *Phys. Lett.* **B696** (2011) 30–39, arXiv:1012.1004 [nucl-ex].
- [8] **ALICE** Collaboration, B. Abelev *et al.*, “Centrality dependence of charged particle production at large transverse momentum in Pb–Pb collisions at $\sqrt{s_{NN}} = 2.76$ TeV,” *Phys. Lett.* **B720** (2013) 52–62, arXiv:1208.2711 [hep-ex].
- [9] **CMS** Collaboration, S. Chatrchyan *et al.*, “Study of high- p_T charged particle suppression in PbPb compared to pp collisions at $\sqrt{s_{NN}} = 2.76$ TeV,” *Eur. Phys. J.* **C72** (2012) 1945, arXiv:1202.2554 [nucl-ex].
- [10] **ATLAS** Collaboration, G. Aad *et al.*, “Measurement of charged-particle spectra in Pb+Pb collisions at $\sqrt{s_{NN}} = 2.76$ TeV with the ATLAS detector at the LHC,” *JHEP* **09** (2015) 050, arXiv:1504.04337 [hep-ex].
- [11] **CMS** Collaboration, V. Khachatryan *et al.*, “Charged-particle nuclear modification factors in PbPb and pPb collisions at $\sqrt{s_{NN}} = 5.02$ TeV,” *JHEP* **04** (2017) 039, arXiv:1611.01664 [nucl-ex].
- [12] **ALICE** Collaboration, B. Abelev *et al.*, “Transverse momentum distribution and nuclear modification factor of charged particles in p+Pb collisions at $\sqrt{s_{NN}} = 5.02$ TeV,” *Phys. Rev. Lett.* **110** (2013) 082302, arXiv:1210.4520 [nucl-ex].
- [13] **ALICE** Collaboration, B. Abelev *et al.*, “Transverse momentum dependence of inclusive primary charged-particle production in p-Pb collisions at $\sqrt{s_{NN}} = 5.02$ TeV,” *Eur. J. Phys.* **C74** (2014) 3054, arXiv:1405.2737 [nucl-ex].
- [14] **CMS** Collaboration, V. Khachatryan *et al.*, “Nuclear effects on the transverse momentum spectra of charged particles in pPb collisions at $\sqrt{s_{NN}} = 5.02$ TeV,” *Eur. Phys. J.* **C75** (2015) 237, arXiv:1502.05387 [nucl-ex].
- [15] **ATLAS** Collaboration, G. Aad *et al.*, “Transverse momentum, rapidity, and centrality dependence of inclusive charged-particle production in $\sqrt{s_{NN}} = 5.02$ TeV p+Pb collisions measured by the ATLAS experiment,” *Phys. Lett.* **B763** (2016) 313–336, arXiv:1605.06436 [hep-ex].
- [16] **ALICE** Collaboration, B. Abelev *et al.*, “Energy dependence of the transverse momentum distributions of charged particles in pp collisions measured by ALICE,” *Eur. Phys. J.* **C73** (2013) 2662, arXiv:1307.1093 [nucl-ex].
- [17] **ALICE** Collaboration, J. Adam *et al.*, “Centrality dependence of the charged-particle multiplicity density at midrapidity in Pb–Pb collisions at $\sqrt{s_{NN}} = 5.02$ TeV,” *Phys. Rev. Lett.* **116** (2016) 222302, arXiv:1512.06104 [nucl-ex].
- [18] **ALICE** Collaboration, K. Aamodt *et al.*, “The ALICE experiment at the CERN LHC,” *JINST* **3** (2008) S08002.
- [19] **ALICE** Collaboration, B. B. Abelev *et al.*, “Performance of the ALICE experiment at the CERN LHC,” *Int. J. Mod. Phys.* **A29** (2014) 1430044, arXiv:1402.4476 [nucl-ex].

- [20] ALICE Collaboration, “ALICE Technical Design Report of the Inner Tracking System (ITS),” Tech. Rep. CERN-LHCC-99-012, CERN, 1999. <http://cds.cern.ch/record/391175>.
- [21] ALICE Collaboration, “ALICE Technical Design Report of the Time Projection Chamber,” Tech. Rep. CERN-LHCC-2000-001, CERN, 2000. <http://cds.cern.ch/record/451098>.
- [22] ALICE Collaboration, “Centrality determination in heavy ion collisions,” Tech. Rep. ALICE-PUBLIC-2018-011, CERN, 2018. <https://cds.cern.ch/record/2636623>.
- [23] ALICE Collaboration, B. Abelev *et al.*, “Measurement of the Cross Section for Electromagnetic Dissociation with Neutron Emission in Pb-Pb Collisions at $\sqrt{s_{NN}} = 2.76$ TeV,” *Phys. Rev. Lett.* **109** (2012) 252302, arXiv:1203.2436 [nucl-ex].
- [24] C. Loizides and A. Morsch, “Absence of jet quenching in peripheral nucleus-nucleus collisions,” *Phys. Lett.* **B773** (2017) 408–411, arXiv:1705.08856 [nucl-ex].
- [25] D. Kharzeev, E. Levin, and M. Nardi, “Color glass condensate at the LHC: Hadron multiplicities in pp, pA and AA collisions,” *Nucl. Phys.* **A747** (2005) 609–629, arXiv:hep-ph/0408050 [hep-ph].
- [26] W.-T. Deng, X.-N. Wang, and R. Xu, “Hadron production in p+p, p+Pb, and Pb+Pb collisions with the HIJING 2.0 model at energies available at the CERN Large Hadron Collider,” *Phys. Rev.* **C83** (2011) 014915, arXiv:1008.1841 [hep-ph].
- [27] ALICE Collaboration, J. Adam *et al.*, “Centrality dependence of particle production in p–Pb Collisions at $\sqrt{s_{NN}} = 5.02$ TeV,” *Phys. Rev. C* **91** (2015) 064905, arXiv:1412.6828 [nucl-ex].
- [28] ALICE Collaboration, “The ALICE definition of primary particles,” Tech. Rep. ALICE-PUBLIC-2017-005, CERN, 2017. <https://cds.cern.ch/record/2270008>.
- [29] ALICE Collaboration, B. Abelev *et al.*, “Measurement of inelastic, single- and double-diffraction cross sections in proton-proton collisions at the LHC with ALICE,” *Eur. Phys. J.* **C73** (2013) 2456, arXiv:1208.4968 [hep-ex].
- [30] ALICE Collaboration, “ALICE luminosity determination for pp collisions at $\sqrt{s} = 5$ TeV,” Tech. Rep. ALICE-PUBLIC-2016-005, CERN, 2016. <https://cds.cern.ch/record/2202638>.
- [31] T. Sjöstrand, S. Mrenna, P. Skands, “A brief introduction to PYTHIA 8.1,” *Comput. Phys. Commun.* **178** (2008) 852–867, arXiv:0710.3820 [hep-ph].
- [32] P. Skands, S. Carrazza, J. Rojo, “Tuning PYTHIA 8.1: the Monash 2013 tune,” *Eur. Phys. J.* **C74** (2014) 3024, arXiv:1404.5630 [hep-ph].
- [33] R. Brun, F. Bruyant, F. Carminati, S. Giani, M. Maire, A. McPherson, G. Patrick, and L. Urban, *GEANT: Detector Description and Simulation Tool; Oct 1994*. CERN Program Library. CERN, Geneva, 1993. <https://cds.cern.ch/record/1082634>. Long Writeup W5013.
- [34] X.-N. Wang and M. Gyulassy, “HIJING: A Monte Carlo model for multiple jet production in p–p, p–A and A–A collisions,” *Phys. Rev.* **D44** (1991) 3501–3516.
- [35] ALICE Collaboration, J. Adam *et al.*, “Measurement of pion, kaon and proton production in proton-proton collisions at $\sqrt{s} = 7$ TeV,” *Eur. Phys. J.* **C75** (2015) 226, arXiv:1504.00024 [nucl-ex].
- [36] ALICE Collaboration, J. Adam *et al.*, “Multiplicity dependence of charged pion, kaon, and (anti)proton production at large transverse momentum in p–Pb Collisions at $\sqrt{s_{NN}} = 5.02$ TeV,” *Phys. Lett.* **B760** (2016) 720–735, arXiv:1601.03658 [nucl-ex].

- [37] **ALICE** Collaboration, J. Adam *et al.*, “Enhanced production of multi-strange hadrons in high-multiplicity proton-proton collisions,” *Nature Physics* **13** (2017) 535–539, arXiv:1606.07424 [nucl-ex].
- [38] **ALICE** Collaboration, B. Abelev *et al.*, “Production of $\Sigma(1385)^\pm$ and $\Xi(1530)^0$ in proton-proton collisions at $\sqrt{s} = 7$ TeV,” *Eur. Phys. J.* **C75** (2015) 1, arXiv:1406.3206 [nucl-ex].
- [39] **ALICE** Collaboration, D. Adamová *et al.*, “Production of $\Sigma(1385)^\pm$ and $\Xi(1530)^0$ in p-Pb collisions at $\sqrt{s_{NN}} = 5.02$ TeV,” *Eur. Phys. J.* **C77** (2017) 389, arXiv:1701.07797 [nucl-ex].
- [40] **ALICE** Collaboration, B. Abelev *et al.*, “Multiplicity Dependence of Pion, Kaon, Proton and Lambda Production in p-Pb Collisions at $\sqrt{s_{NN}} = 5.02$ TeV,” *Phys. Lett.* **B728** (2014) 25–38, arXiv:1307.6796 [nucl-ex].
- [41] **ALICE** Collaboration, B. Abelev *et al.*, “Centrality dependence of π , K, p production in Pb-Pb collisions at $\sqrt{s_{NN}} = 2.76$ TeV,” *Phys. Rev.* **C88** (2013) 044910, arXiv:1303.0737 [hep-ex].
- [42] **ALICE** Collaboration, B. Abelev *et al.*, “ K_S^0 and Λ production in Pb-Pb collisions at $\sqrt{s_{NN}} = 2.76$ TeV,” *Phys. Rev. Lett.* **111** (2013) 222301, arXiv:1307.5530 [nucl-ex].
- [43] **ALICE** Collaboration, B. Abelev *et al.*, “Production of charged pions, kaons and protons at large transverse momenta in pp and Pb-Pb collisions at $\sqrt{s_{NN}} = 2.76$ TeV,” *Phys. Lett.* **B736** (2014) 196–207, arXiv:1401.1250 [nucl-ex].
- [44] **ALICE** Collaboration, J. Adam *et al.*, “Centrality dependence of the nuclear modification factor of charged pions, kaons, and protons in Pb-Pb collisions at $\sqrt{s_{NN}} = 2.76$ TeV,” *Phys. Rev.* **C93** (2016) 034913, arXiv:1506.07287 [nucl-ex].
- [45] A. A. Bylinkin and A. A. Rostovtsev, “Parametrization of the shape of hadron-production spectra in high-energy particle interactions,” *Phys. Atom. Nucl.* **88** (2012) 999–1005.
- [46] D. de Florian, M. Epele, R. J. Hernandez-Pinto, R. Sassot, and M. Stratmann, “Parton-to-Kaon Fragmentation Revisited,” *Phys. Rev.* **D95** (2017) 094019, arXiv:1702.06353 [hep-ph].
- [47] S. Roesler, R. Engel, and J. Ranft, “The Monte Carlo event generator DPMJET-III,” in *Advanced Monte Carlo for radiation physics, particle transport simulation and applications. Proceedings, Conference, MC2000, Lisbon, Portugal, October 23-26, 2000*, pp. 1033–1038. 2000. arXiv:hep-ph/0012252 [hep-ph]. <http://www-public.slac.stanford.edu/sciDoc/docMeta.aspx?slacPubNumber=SLAC-PUB-8740>.
- [48] E. Schnedermann, J. Sollfrank, and U. W. Heinz, “Thermal phenomenology of hadrons from 200-A/GeV S+S collisions,” *Phys. Rev.* **C48** (1993) 2462–2475, arXiv:nucl-th/9307020 [nucl-th].
- [49] G. D’Agostini, “A Multidimensional unfolding method based on Bayes’ theorem,” *Nucl. Instrum. Meth.* **A362** (1995) 487–498.
- [50] T. Auye, “Unfolding algorithms and tests using RooUnfold,” in *Proceedings, PHYSTAT 2011 Workshop on Statistical Issues Related to Discovery Claims in Search Experiments and Unfolding, CERN, Geneva, Switzerland 17-20 January 2011*, pp. 313–318, CERN. CERN, Geneva, 2011. arXiv:1105.1160 [physics.data-an]. <https://inspirehep.net/record/898599/files/arXiv:1105.1160.pdf>.
- [51] R. Hagedorn, “Multiplicities, p_T distributions and the expected hadron \rightarrow quark-gluon phase transition,” *Riv. Nuovo Cim.* **6** (1983) 1–50.

- [52] Z.-W. Lin, C. M. Ko, B.-A. Li, B. Zhang, and S. Pal, “A Multi-phase transport model for relativistic heavy ion collisions,” *Phys. Rev.* **C72** (2005) 064901, arXiv:nuc1-th/0411110 [nucl-th].
- [53] T. Pierog, I. Karpenko, J. Katzy, E. Yatsenko, and K. Werner, “EPOS LHC: Test of collective hadronization with data measured at the CERN Large Hadron Collider,” *Phys. Rev.* **C92** (2015) 034906, arXiv:1306.0121 [hep-ph].
- [54] J. W. Cronin, H. J. Frisch, M. J. Shochet, J. P. Boymond, R. Mermod, P. A. Piroué, and R. L. Sumner, “Production of hadrons with large transverse momentum at 200, 300, and 400 GeV,” *Phys. Rev.* **D11** (1975) 3105–3123.
- [55] Z.-B. Kang, R. Lashof-Regas, G. Ovanesyan, P. Saad, and I. Vitev, “Jet quenching phenomenology from soft-collinear effective theory with Glauber gluons,” *Phys. Rev. Lett.* **114** (2015) 092002, arXiv:1405.2612 [hep-ph].
- [56] Y.-T. Chien, A. Emerman, Z.-B. Kang, G. Ovanesyan, and I. Vitev, “Jet quenching from QCD evolution,” *Phys. Rev.* **D93** (2016) 074030, arXiv:1509.02936 [hep-ph].
- [57] M. Djordjevic and M. Djordjevic, “Predictions of heavy-flavor suppression at 5.1 TeV Pb+Pb collisions at the CERN Large Hadron Collider,” *Phys. Rev.* **C92** (2016) 024918, arXiv:1505.04316 [nucl-th].
- [58] M. Djordjevic, B. Blagojevic, and L. Zivkovic, “Mass tomography at different momentum ranges in quark-gluon plasma,” *Phys. Rev.* **C94** (2016) 044908, arXiv:1601.07852 [nucl-th].
- [59] E. Bianchi, J. Elledge, A. Kumar, A. Majumder, G.-Y. Qin, and C. Shen, “The x and Q^2 dependence of \hat{q} , quasi-particles and the JET puzzle,” arXiv:1702.00481 [nucl-th].
- [60] J. Xu, J. Liao, and M. Gyulassy, “Consistency of perfect fluidity and jet quenching in semi-quark-gluon monopole plasmas,” *Chin. Phys. Lett.* **32** (2015) 092501, arXiv:1411.3673 [hep-ph].
- [61] J. Xu, J. Liao, and M. Gyulassy, “Bridging soft-hard transport properties of quark-gluon plasmas with CUJET3.0,” *JHEP* **02** (2016) 169, arXiv:1508.00552 [hep-ph].
- [62] C. Andrés, N. Armesto, M. Luzum, C. A. Salgado, and P. Zurita, “Energy versus centrality dependence of the jet quenching parameter \hat{q} at RHIC and LHC: a new puzzle?,” *Eur. Phys. J.* **C76** (2016) 475, arXiv:1606.04837 [hep-ph].
- [63] R. Baier, “Jet quenching,” *Nucl. Phys.* **A715** (2003) 209–218, arXiv:hep-ph/0209038 [hep-ph].

A The ALICE Collaboration

S. Acharya¹³⁹, F.T.-. Acosta²², D. Adamová⁹⁴, J. Adolfsson⁸¹, M.M. Aggarwal⁹⁸, G. Aglieri Rinella³⁶, M. Agnello³³, N. Agrawal⁴⁸, Z. Ahammed¹³⁹, S.U. Ahn⁷⁷, S. Aiola¹⁴⁴, A. Akhmedov⁶⁴, M. Al-Turany¹⁰⁴, S.N. Alam¹³⁹, D.S.D. Albuquerque¹²⁰, D. Aleksandrov⁸⁸, B. Alessandro⁵⁸, R. Alfaro Molina⁷², Y. Ali¹⁶, A. Alici^{11, 53, 29}, A. Alkin³, J. Alme²⁴, T. Alt⁶⁹, L. Altenkamper²⁴, I. Altsybeev¹³⁸, C. Andrei⁴⁷, D. Andreou³⁶, H.A. Andrews¹⁰⁸, A. Andronic¹⁰⁴, M. Angeletti³⁶, V. Anguelov¹⁰², C. Anson¹⁷, T. Antičić¹⁰⁵, F. Antinori⁵⁶, P. Antonioli⁵³, N. Apadula⁸⁰, L. Aphecetche¹¹², H. Appelshäuser⁶⁹, S. Arcelli²⁹, R. Arnaldi⁵⁸, O.W. Arnold^{103, 115}, I.C. Arsene²³, M. Arslandok¹⁰², B. Audurier¹¹², A. Augustinus³⁶, R. Averbeck¹⁰⁴, M.D. Azmi¹⁸, A. Badalá⁵⁵, Y.W. Baek^{60, 76}, S. Bagnasco⁵⁸, R. Bailhache⁶⁹, R. Bala⁹⁹, A. Baldisseri¹³⁵, M. Ball⁴³, R.C. Baral⁸⁶, A.M. Barbano²⁸, R. Barbera³⁰, F. Barile⁵², L. Barioglio²⁸, G.G. Barnaföldi¹⁴³, L.S. Barnby⁹³, V. Barret¹³², P. Bartalini⁷, K. Barth³⁶, E. Bartsch⁶⁹, N. Bastid¹³², S. Basu¹⁴¹, G. Batigne¹¹², B. Batyunya⁷⁵, P.C. Batzing²³, J.L. Bazo Alba¹⁰⁹, I.G. Bearden⁸⁹, H. Beck¹⁰², C. Bedda⁶³, N.K. Behera⁶⁰, I. Belikov¹³⁴, F. Bellini^{29, 36}, H. Bello Martinez², R. Bellwied¹²⁴, L.G.E. Beltran¹¹⁸, V. Belyaev⁹², G. Bencedi¹⁴³, S. Beole²⁸, A. Bercuci⁴⁷, Y. Berdnikov⁹⁶, D. Berenyi¹⁴³, R.A. Bertens¹²⁸, D. Berzano^{36, 58}, L. Betev³⁶, P.P. Bhaduri¹³⁹, A. Bhasin⁹⁹, I.R. Bhat⁹⁹, B. Bhattacharjee⁴², J. Bhom¹¹⁶, A. Bianchi²⁸, L. Bianchi¹²⁴, N. Bianchi⁵¹, J. Bielčák³⁸, J. Bielčiková⁹⁴, A. Bilandzic^{103, 115}, G. Biro¹⁴³, R. Biswas⁴, S. Biswas⁴, J.T. Blair¹¹⁷, D. Blau⁸⁸, C. Blume⁶⁹, G. Boca¹³⁶, F. Bock³⁶, A. Bogdanov⁹², L. Boldizsár¹⁴³, M. Bombara³⁹, G. Bonomi¹³⁷, M. Bonora³⁶, H. Borel¹³⁵, A. Borissov²⁰, M. Borri¹²⁶, E. Botta²⁸, C. Bourjau⁸⁹, L. Bratrud⁶⁹, P. Braun-Munzinger¹⁰⁴, M. Bregant¹¹⁹, T.A. Broker⁶⁹, M. Broz³⁸, E.J. Brucken⁴⁴, E. Bruna⁵⁸, G.E. Bruno^{36, 35}, D. Budnikov¹⁰⁶, H. Buesching⁶⁹, S. Bufalino³³, P. Buhler¹¹¹, P. Buncic³⁶, O. Busch¹³¹, Z. Buthelezi⁷³, J.B. Butt¹⁶, J.T. Buxton¹⁹, J. Cabala¹¹⁴, D. Caffarri^{36, 90}, H. Caines¹⁴⁴, A. Caliva¹⁰⁴, E. Calvo Villar¹⁰⁹, R.S. Camacho², P. Camerini²⁷, A.A. Capon¹¹¹, F. Carena³⁶, W. Carena³⁶, F. Carnesecchi^{11, 29}, J. Castillo Castellanos¹³⁵, A.J. Castro¹²⁸, E.A.R. Casula⁵⁴, C. Ceballos Sanchez⁹, S. Chandra¹³⁹, B. Chang¹²⁵, W. Chang⁷, S. Chapeland³⁶, M. Chartier¹²⁶, S. Chattopadhyay¹³⁹, S. Chattopadhyay¹⁰⁷, A. Chauvin^{115, 103}, C. Cheshkov¹³³, B. Cheynis¹³³, V. Chibante Barroso³⁶, D.D. Chinellato¹²⁰, S. Cho⁶⁰, P. Chochula³⁶, S. Choudhury¹³⁹, T. Chowdhury¹³², P. Christakoglou⁹⁰, C.H. Christensen⁸⁹, P. Christiansen⁸¹, T. Chujo¹³¹, S.U. Chung²⁰, C. Cicalo⁵⁴, L. Cifarelli^{11, 29}, F. Cindolo⁵³, J. Cleymans¹²³, F. Colamaria^{52, 35}, D. Colella^{36, 52, 65}, A. Collu⁸⁰, M. Colocci²⁹, M. Concas^{58, ii}, G. Conesa Balbastre⁷⁹, Z. Conesa de Valle⁶¹, J.G. Contreras³⁸, T.M. Cormier⁹⁵, Y. Corrales Morales⁵⁸, I. Cortés Maldonado², P. Cortese³⁴, M.R. Cosentino¹²¹, F. Costa³⁶, S. Costanza¹³⁶, J. Crkovská⁶¹, P. Crochet¹³², E. Cuautle⁷⁰, L. Cunqueiro^{95, 142}, T. Dahms^{115, 103}, A. Dainese⁵⁶, M.C. Danisch¹⁰², A. Danu⁶⁸, D. Das¹⁰⁷, I. Das¹⁰⁷, S. Das⁴, A. Dash⁸⁶, S. Dash⁴⁸, S. De⁴⁹, A. De Caro³², G. de Cataldo⁵², C. de Conti¹¹⁹, J. de Cuveland⁴⁰, A. De Falco²⁶, D. De Gruttola^{32, 11}, N. De Marco⁵⁸, S. De Pasquale³², R.D. De Souza¹²⁰, H.F. Degenhardt¹¹⁹, A. Deisting^{104, 102}, A. Deloff⁸⁵, S. Delsanto²⁸, C. Deplano⁹⁰, P. Dhankher⁴⁸, D. Di Bari³⁵, A. Di Mauro³⁶, B. Di Ruzza⁵⁶, R.A. Diaz⁹, T. Dietel¹²³, P. Dillenseger⁶⁹, Y. Ding⁷, R. Divià³⁶, Ø. Djuvsland²⁴, A. Dobrin³⁶, D. Domenicis Gimenez¹¹⁹, B. Dönigus⁶⁹, O. Dordic²³, L.V.R. Doremalen⁶³, A.K. Dubey¹³⁹, A. Dubla¹⁰⁴, L. Ducroux¹³³, S. Dudi⁹⁸, A.K. Duggal⁹⁸, M. Dukhishyam⁸⁶, P. Dupieux¹³², R.J. Ehlers¹⁴⁴, D. Elia⁵², E. Endress¹⁰⁹, H. Engel⁷⁴, E. Epple¹⁴⁴, B. Erazmus¹¹², F. Erhardt⁹⁷, M.R. Ersdal²⁴, B. Espagnon⁶¹, G. Eulisse³⁶, J. Eum²⁰, D. Evans¹⁰⁸, S. Evdokimov⁹¹, L. Fabbietti^{103, 115}, M. Faggin³¹, J. Faivre⁷⁹, A. Fantoni⁵¹, M. Fasel⁹⁵, L. Feldkamp¹⁴², A. Feliciello⁵⁸, G. Feofilov¹³⁸, A. Fernández Téllez², A. Ferretti²⁸, A. Festanti^{31, 36}, V.J.G. Feuillard^{135, 132}, J. Figiel¹¹⁶, M.A.S. Figueredo¹¹⁹, S. Filchagin¹⁰⁶, D. Finogeev⁶², F.M. Fionda^{24, 26}, M. Floris³⁶, S. Foertsch⁷³, P. Foka¹⁰⁴, S. Fokin⁸⁸, E. Fragiaco⁵⁹, A. Francescon³⁶, A. Francisco¹¹², U. Frankenfeld¹⁰⁴, G.G. Fronze²⁸, U. Fuchs³⁶, C. Furget⁷⁹, A. Furs⁶², M. Fusco Girard³², J.J. Gaardhøje⁸⁹, M. Gagliardi²⁸, A.M. Gago¹⁰⁹, K. Gajdosova⁸⁹, M. Gallio²⁸, C.D. Galvan¹¹⁸, P. Ganoti⁸⁴, C. Garabatos¹⁰⁴, E. Garcia-Solis¹², K. Garg³⁰, C. Gargiulo³⁶, P. Gasik^{115, 103}, E.F. Gauger¹¹⁷, M.B. Gay Ducati⁷¹, M. Germain¹¹², J. Ghosh¹⁰⁷, P. Ghosh¹³⁹, S.K. Ghosh⁴, P. Gianotti⁵¹, P. Giubellino^{104, 58}, P. Giubilato³¹, P. Glässel¹⁰², D.M. Gómez Coral⁷², A. Gomez Ramirez⁷⁴, V. Gonzalez¹⁰⁴, P. González-Zamora², S. Gorbunov⁴⁰, L. Görlich¹¹⁶, S. Gotovac¹²⁷, V. Grabski⁷², L.K. Graczykowski¹⁴⁰, K.L. Graham¹⁰⁸, L. Greiner⁸⁰, A. Grelli⁶³, C. Grigoras³⁶, V. Grigoriev⁹², A. Grigoryan¹, S. Grigoryan⁷⁵, J.M. Gronefeld¹⁰⁴, F. Grosa³³, J.F. Grosse-Oetringhaus³⁶, R. Grosso¹⁰⁴, R. Guernane⁷⁹, B. Guerzoni²⁹, M. Guittiere¹¹², K. Gulbrandsen⁸⁹, T. Gunji¹³⁰, A. Gupta⁹⁹, R. Gupta⁹⁹, I.B. Guzman², R. Haake³⁶, M.K. Habib¹⁰⁴, C. Hadjidakís⁶¹, H. Hamagaki⁸², G. Hamar¹⁴³, J.C. Hamon¹³⁴, M.R. Haque⁶³, J.W. Harris¹⁴⁴, A. Harton¹², H. Hassan⁷⁹, D. Hatzifotiadou^{53, 11}, S. Hayashi¹³⁰, S.T. Heckel⁶⁹, E. Hellbär⁶⁹, H. Helstrup³⁷, A. Hergelegiu⁴⁷, E.G. Hernandez², G. Herrera Corral¹⁰, F. Herrmann¹⁴², K.F. Hetland³⁷, T.E. Hilden⁴⁴, H. Hillemanns³⁶, C. Hills¹²⁶, B. Hippolyte¹³⁴, B. Hohlweger¹⁰³, D. Horak³⁸, S. Hornung¹⁰⁴, R. Hosokawa^{131, 79}, P. Hristov³⁶, C. Hughes¹²⁸, P. Huhn⁶⁹, T.J. Humanic¹⁹, H. Hushnud¹⁰⁷, N. Hussain⁴²,

T. Hussain¹⁸, D. Hutter⁴⁰, D.S. Hwang²¹, J.P. Iddon¹²⁶, S.A. Iga Buitron⁷⁰, R. Ilkaev¹⁰⁶, M. Inaba¹³¹, M. Ippolitov^{92,88}, M.S. Islam¹⁰⁷, M. Ivanov¹⁰⁴, V. Ivanov⁹⁶, V. Izucheev⁹¹, B. Jacak⁸⁰, N. Jacazio²⁹, P.M. Jacobs⁸⁰, M.B. Jadhav⁴⁸, S. Jadlovská¹¹⁴, J. Jadlovsky¹¹⁴, S. Jaelani⁶³, C. Jahnke^{115,119}, M.J. Jakubowska¹⁴⁰, M.A. Janik¹⁴⁰, P.H.S.Y. Jayarathna¹²⁴, C. Jena⁸⁶, M. Jercic⁹⁷, R.T. Jimenez Bustamante¹⁰⁴, P.G. Jones¹⁰⁸, A. Jusko¹⁰⁸, P. Kalinak⁶⁵, A. Kalweit³⁶, J.H. Kang¹⁴⁵, V. Kaplin⁹², S. Kar^{7,139}, A. Karasu Uysal⁷⁸, O. Karavichev⁶², T. Karavicheva⁶², L. Karayan^{104,102}, P. Karczmarczyk³⁶, E. Karpechev⁶², U. Kebschull⁷⁴, R. Keidel⁴⁶, D.L.D. Keijdener⁶³, M. Keil³⁶, B. Ketzer⁴³, Z. Khabanova⁹⁰, S. Khan¹⁸, S.A. Khan¹³⁹, A. Khanzadeev⁹⁶, Y. Kharlov⁹¹, A. Khatun¹⁸, A. Khuntia⁴⁹, M.M. Kielbowicz¹¹⁶, B. Kileng³⁷, B. Kim¹³¹, D. Kim¹⁴⁵, D.J. Kim¹²⁵, E.J. Kim¹⁴, H. Kim¹⁴⁵, J.S. Kim⁴¹, J. Kim¹⁰², M. Kim⁶⁰, S. Kim²¹, T. Kim¹⁴⁵, T. Kim¹⁴⁵, S. Kirsch⁴⁰, I. Kisel⁴⁰, S. Kiselev⁶⁴, A. Kisiel¹⁴⁰, G. Kiss¹⁴³, J.L. Klay⁶, C. Klein⁶⁹, J. Klein^{36,58}, C. Klein-Bösing¹⁴², S. Klewin¹⁰², A. Kluge³⁶, M.L. Knichel^{102,36}, A.G. Knospe¹²⁴, C. Kobdaj¹¹³, M. Kofarago¹⁴³, M.K. Köhler¹⁰², T. Kollegger¹⁰⁴, V. Kondratiev¹³⁸, N. Kondratyeva⁹², E. Kondratyuk⁹¹, A. Konevskikh⁶², M. Konyushikhin¹⁴¹, O. Kovalenko⁸⁵, V. Kovalenko¹³⁸, M. Kowalski¹¹⁶, I. Králik⁶⁵, A. Kravčáková³⁹, L. Kreis¹⁰⁴, M. Krivda^{65,108}, F. Krizek⁹⁴, M. Krüger⁶⁹, E. Kryshen⁹⁶, M. Krzewicki⁴⁰, A.M. Kubera¹⁹, V. Kučera^{94,60}, C. Kuhn¹³⁴, P.G. Kuijter⁹⁰, J. Kumar⁴⁸, L. Kumar⁹⁸, S. Kumar⁴⁸, S. Kundu⁸⁶, P. Kurashvili⁸⁵, A. Kurepin⁶², A.B. Kurepin⁶², A. Kuryakin¹⁰⁶, S. Kuschpil⁹⁴, M.J. Kweon⁶⁰, Y. Kwon¹⁴⁵, S.L. La Pointe⁴⁰, P. La Rocca³⁰, C. Lagana Fernandes¹¹⁹, Y.S. Lai⁸⁰, I. Lakomov³⁶, R. Langoy¹²², K. Lapidus¹⁴⁴, C. Lara⁷⁴, A. Lardeux²³, P. Larionov⁵¹, A. Lattuca²⁸, E. Laudi³⁶, R. Lavicka³⁸, R. Lea²⁷, L. Leardini¹⁰², S. Lee¹⁴⁵, F. Lehas⁹⁰, S. Lehner¹¹¹, J. Lehrbach⁴⁰, R.C. Lemmon⁹³, E. Leogrande⁶³, I. León Monzón¹¹⁸, P. Lévai¹⁴³, X. Li¹³, X.L. Li⁷, J. Lien¹²², R. Lietava¹⁰⁸, B. Lim²⁰, S. Lindal²³, V. Lindenstruth⁴⁰, S.W. Lindsay¹²⁶, C. Lippmann¹⁰⁴, M.A. Lisa¹⁹, V. Litichevskyi⁴⁴, A. Liu⁸⁰, H.M. Ljunggren⁸¹, W.J. Llope¹⁴¹, D.F. Lodato⁶³, V. Loginov⁹², C. Loizides^{95,80}, P. Loncar¹²⁷, X. Lopez¹³², E. López Torres⁹, A. Lowe¹⁴³, P. Luettig⁶⁹, J.R. Luhder¹⁴², M. Lunardon³¹, G. Luparello⁵⁹, M. Lupi³⁶, A. Maevskaya⁶², M. Mager³⁶, S.M. Mahmood²³, A. Maire¹³⁴, R.D. Majka¹⁴⁴, M. Malaev⁹⁶, L. Malinina^{75,iii}, D. Mal'Kevich⁶⁴, P. Malzacher¹⁰⁴, A. Mamonov¹⁰⁶, V. Manko⁸⁸, F. Manso¹³², V. Manzari⁵², Y. Mao⁷, M. Marchisone^{129,73,133}, J. Mareš⁶⁷, G.V. Margagliotti²⁷, A. Margotti⁵³, J. Margutti⁶³, A. Marín¹⁰⁴, C. Markert¹¹⁷, M. Marquard⁶⁹, N.A. Martin¹⁰⁴, P. Martinengo³⁶, M.I. Martínez², G. Martínez García¹¹², M. Martinez Pedreira³⁶, S. Masciocchi¹⁰⁴, M. Maserà²⁸, A. Masoni⁵⁴, L. Massacrier⁶¹, E. Masson¹¹², A. Mastroserio⁵², A.M. Mathis^{103,115}, P.F.T. Matuoka¹¹⁹, A. Matyja¹²⁸, C. Mayer¹¹⁶, M. Mazzilli³⁵, M.A. Mazzoni⁵⁷, F. Meddi²⁵, Y. Melikyan⁹², A. Menchaca-Rocha⁷², J. Mercado Pérez¹⁰², M. Meres¹⁵, C.S. Meza¹⁰⁹, S. Mhlanga¹²³, Y. Miake¹³¹, L. Micheletti²⁸, M.M. Mieskolainen⁴⁴, D.L. Mihaylov¹⁰³, K. Mikhaylov^{64,75}, A. Mischke⁶³, A.N. Mishra⁷⁰, D. Miśkowiec¹⁰⁴, J. Mitra¹³⁹, C.M. Mitu⁶⁸, N. Mohammadi^{36,63}, A.P. Mohanty⁶³, B. Mohanty⁸⁶, M. Mohisin Khan^{18,iv}, D.A. Moreira De Godoy¹⁴², L.A.P. Moreno², S. Moretto³¹, A. Morreale¹¹², A. Morsch³⁶, V. Muccifora⁵¹, E. Mudnic¹²⁷, D. Mühlheim¹⁴², S. Muhuri¹³⁹, M. Mukherjee⁴, J.D. Mulligan¹⁴⁴, M.G. Munhoz¹¹⁹, K. Münnig⁴³, M.I.A. Muñoz⁸⁰, R.H. Munzer⁶⁹, H. Murakami¹³⁰, S. Murray⁷³, L. Musa³⁶, J. Musinsky⁶⁵, C.J. Myers¹²⁴, J.W. Myrcha¹⁴⁰, B. Naik⁴⁸, R. Nair⁸⁵, B.K. Nandi⁴⁸, R. Nania^{53,11}, E. Nappi⁵², A. Narayan⁴⁸, M.U. Naru¹⁶, H. Natal da Luz¹¹⁹, C. Natrass¹²⁸, S.R. Navarro², K. Nayak⁸⁶, R. Nayak⁴⁸, T.K. Nayak¹³⁹, S. Nazarenko¹⁰⁶, R.A. Negrao De Oliveira^{69,36}, L. Nellen⁷⁰, S.V. Nesbo³⁷, G. Neskovic⁴⁰, F. Ng¹²⁴, M. Nicassio¹⁰⁴, J. Niedziela^{140,36}, B.S. Nielsen⁸⁹, S. Nikolaev⁸⁸, S. Nikulin⁸⁸, V. Nikulin⁹⁶, F. Noferini^{11,53}, P. Nomokonov⁷⁵, G. Nooren⁶³, J.C.C. Noris², J. Norman^{79,126}, A. Nyanin⁸⁸, J. Nystrand²⁴, H. Oeschler^{20,102,i}, H. Oh¹⁴⁵, A. Ohlson¹⁰², L. Olah¹⁴³, J. Oleniacz¹⁴⁰, A.C. Oliveira Da Silva¹¹⁹, M.H. Oliver¹⁴⁴, J. Onderwaater¹⁰⁴, C. Oppedisano⁵⁸, R. Orava⁴⁴, M. Oravec¹¹⁴, A. Ortiz Velasquez⁷⁰, A. Oskarsson⁸¹, J. Otwinowski¹¹⁶, K. Oyama⁸², Y. Pachmayer¹⁰², V. Pacik⁸⁹, D. Pagano¹³⁷, G. Paic⁷⁰, P. Palni⁷, J. Pan¹⁴¹, A.K. Pandey⁴⁸, S. Panebianco¹³⁵, V. Papikyan¹, P. Pareek⁴⁹, J. Park⁶⁰, S. Parmar⁹⁸, A. Passfeld¹⁴², S.P. Pathak¹²⁴, R.N. Patra¹³⁹, B. Paul⁵⁸, H. Pei⁷, T. Peitzmann⁶³, X. Peng⁷, L.G. Pereira⁷¹, H. Pereira Da Costa¹³⁵, D. Peresunko^{92,88}, E. Perez Lezama⁶⁹, V. Peskov⁶⁹, Y. Pestov⁵, V. Petráček³⁸, M. Petrovici⁴⁷, C. Petta³⁰, R.P. Pezzi⁷¹, S. Piano⁵⁹, M. Pikna¹⁵, P. Pillot¹¹², L.O.D.L. Pimentel⁸⁹, O. Pinazza^{53,36}, L. Pinsky¹²⁴, S. Pisano⁵¹, D.B. Piyarathna¹²⁴, M. Płoskoń⁸⁰, M. Planinic⁹⁷, F. Pliquett⁶⁹, J. Pluta¹⁴⁰, S. Pochybova¹⁴³, P.L.M. Podesta-Lerma¹¹⁸, M.G. Poghosyan⁹⁵, B. Polichtchouk⁹¹, N. Poljak⁹⁷, W. Poonsawat¹¹³, A. Pop⁴⁷, H. Poppenborg¹⁴², S. Porteboeuf-Houssais¹³², V. Pozdniakov⁷⁵, S.K. Prasad⁴, R. Preghenella⁵³, F. Prino⁵⁸, C.A. Pruneau¹⁴¹, I. Pshenichnov⁶², M. Puccio²⁸, V. Punin¹⁰⁶, J. Putschke¹⁴¹, S. Raha⁴, S. Rajput⁹⁹, J. Rak¹²⁵, A. Rakotozafindrabe¹³⁵, L. Ramello³⁴, F. Rami¹³⁴, D.B. Rana¹²⁴, R. Raniwala¹⁰⁰, S. Raniwala¹⁰⁰, S.S. Räsänen⁴⁴, B.T. Rascanu⁶⁹, D. Rathee⁹⁸, V. Ratzka⁴³, I. Ravasenga³³, K.F. Read^{128,95}, K. Redlich^{85,v}, A. Rehman²⁴, P. Reichelt⁶⁹, F. Reidt³⁶, X. Ren⁷, R. Renfordt⁶⁹, A. Reshetin⁶², J.-P. Revol¹¹, K. Reygers¹⁰², V. Riabov⁹⁶, T. Richert^{63,81}, M. Richter²³, P. Riedler³⁶, W. Riegler³⁶, F. Riggi³⁰, C. Ristea⁶⁸, M. Rodríguez

Cahuantzi², K. Røed²³, R. Rogalev⁹¹, E. Rogochaya⁷⁵, D. Rohr³⁶, D. Röhrich²⁴, P.S. Rokita¹⁴⁰, F. Ronchetti⁵¹, E.D. Rosas⁷⁰, K. Roslon¹⁴⁰, P. Rosnet¹³², A. Rossi^{56,31}, A. Rotondi¹³⁶, F. Roukoutakis⁸⁴, C. Roy¹³⁴, P. Roy¹⁰⁷, O.V. Rueda⁷⁰, R. Rui²⁷, B. Rumyantsev⁷⁵, A. Rustamov⁸⁷, E. Ryabinkin⁸⁸, Y. Ryabov⁹⁶, A. Rybicki¹¹⁶, S. Saarinen⁴⁴, S. Sadhu¹³⁹, S. Sadovsky⁹¹, K. Šafařík³⁶, S.K. Saha¹³⁹, B. Sahoo⁴⁸, P. Sahoo⁴⁹, R. Sahoo⁴⁹, S. Sahoo⁶⁶, P.K. Sahu⁶⁶, J. Saini¹³⁹, S. Sakai¹³¹, M.A. Saleh¹⁴¹, S. Sambyal⁹⁹, V. Samsonov^{96,92}, A. Sandoval⁷², A. Sarkar⁷³, D. Sarkar¹³⁹, N. Sarkar¹³⁹, P. Sarma⁴², M.H.P. Sas⁶³, E. Scapparone⁵³, F. Scarlassara³¹, B. Schaefer⁹⁵, H.S. Scheid⁶⁹, C. Schiaua⁴⁷, R. Schicker¹⁰², C. Schmidt¹⁰⁴, H.R. Schmidt¹⁰¹, M.O. Schmidt¹⁰², M. Schmidt¹⁰¹, N.V. Schmidt^{95,69}, J. Schukraft³⁶, Y. Schutz^{36,134}, K. Schwarz¹⁰⁴, K. Schweda¹⁰⁴, G. Scioli²⁹, E. Scomparin⁵⁸, M. Šefčík³⁹, J.E. Seger¹⁷, Y. Sekiguchi¹³⁰, D. Sekihata⁴⁵, I. Selyuzhenkov^{92,104}, K. Senosi⁷³, S. Senyukov¹³⁴, E. Serradilla⁷², P. Sett⁴⁸, A. Sevcenco⁶⁸, A. Shabanov⁶², A. Shabetai¹¹², R. Shahoyan³⁶, W. Shaikh¹⁰⁷, A. Shangaraev⁹¹, A. Sharma⁹⁸, A. Sharma⁹⁹, N. Sharma⁹⁸, A.I. Sheikh¹³⁹, K. Shigaki⁴⁵, M. Shimomura⁸³, S. Shirinkin⁶⁴, Q. Shou^{110,7}, K. Shtejer²⁸, Y. Sibiriak⁸⁸, S. Siddhanta⁵⁴, K.M. Sielewicz³⁶, T. Siemiarczuk⁸⁵, S. Silaeva⁸⁸, D. Silvermyr⁸¹, G. Simatovic⁹⁰, G. Simonetti^{36,103}, R. Singaraju¹³⁹, R. Singh⁸⁶, V. Singhal¹³⁹, T. Sinha¹⁰⁷, B. Sitar¹⁵, M. Sitta³⁴, T.B. Skaali²³, M. Slupecki¹²⁵, N. Smirnov¹⁴⁴, R.J.M. Snellings⁶³, T.W. Snellman¹²⁵, J. Song²⁰, F. Soramel³¹, S. Sorensen¹²⁸, F. Sozzi¹⁰⁴, I. Sputowska¹¹⁶, J. Stachel¹⁰², I. Stan⁶⁸, P. Stankus⁹⁵, E. Stenlund⁸¹, D. Stocco¹¹², M.M. Storetvedt³⁷, P. Strmen¹⁵, A.A.P. Suaide¹¹⁹, T. Sugitate⁴⁵, C. Suire⁶¹, M. Suleymanov¹⁶, M. Suljic^{36,27}, R. Sultanov⁶⁴, M. Šumbera⁹⁴, S. Sumowidagdo⁵⁰, K. Suzuki¹¹¹, S. Swain⁶⁶, A. Szabo¹⁵, I. Szarka¹⁵, U. Tabassam¹⁶, J. Takahashi¹²⁰, G.J. Tambave²⁴, N. Tanaka¹³¹, M. Tarhini^{61,112}, M. Tariq¹⁸, M.G. Tarzila⁴⁷, A. Tauro³⁶, G. Tejada Muñoz², A. Telesca³⁶, C. Terrevoli³¹, B. Teyssier¹³³, D. Thakur⁴⁹, S. Thakur¹³⁹, D. Thomas¹¹⁷, F. Thoresen⁸⁹, R. Tieulent¹³³, A. Tikhonov⁶², A.R. Timmins¹²⁴, A. Toia⁶⁹, N. Topilskaya⁶², M. Toppi⁵¹, S.R. Torres¹¹⁸, S. Tripathy⁴⁹, S. Trogolo²⁸, G. Trombetta³⁵, L. Tropp³⁹, V. Trubnikov³, W.H. Trzaska¹²⁵, T.P. Trzcinski¹⁴⁰, B.A. Trzeciak⁶³, T. Tsuji¹³⁰, A. Tumkin¹⁰⁶, R. Turrisi⁵⁶, T.S. Tveter²³, K. Ullaland²⁴, E.N. Umaka¹²⁴, A. Uras¹³³, G.L. Usai²⁶, A. Utrobicic⁹⁷, M. Vala¹¹⁴, J. Van Der Maarel⁶³, J.W. Van Hoorne³⁶, M. van Leeuwen⁶³, T. Vanat⁹⁴, P. Vande Vyvre³⁶, D. Varga¹⁴³, A. Vargas², M. Vargyas¹²⁵, R. Varma⁴⁸, M. Vasileiou⁸⁴, A. Vasiliev⁸⁸, A. Vauthier⁷⁹, O. Vázquez Doce^{115,103}, V. Vechernin¹³⁸, A.M. Veen⁶³, A. Velure²⁴, E. Vercellin²⁸, S. Vergara Limón², L. Vermunt⁶³, R. Vernet⁸, R. Vértesi¹⁴³, L. Vickovic¹²⁷, J. Viinikainen¹²⁵, Z. Vilakazi¹²⁹, O. Villalobos Baillie¹⁰⁸, A. Villatoro Tello², A. Vinogradov⁸⁸, L. Vinogradov¹³⁸, T. Virgili³², V. Visklavicius⁸¹, A. Vodopyanov⁷⁵, M.A. Völkl¹⁰¹, K. Voloshin⁶⁴, S.A. Voloshin¹⁴¹, G. Volpe³⁵, B. von Haller³⁶, I. Vorobyev^{115,103}, D. Voscek¹¹⁴, D. Vranic^{36,104}, J. Vrláková³⁹, B. Wagner²⁴, H. Wang⁶³, M. Wang⁷, Y. Watanabe^{130,131}, M. Weber¹¹¹, S.G. Weber¹⁰⁴, A. Wegrzynek³⁶, D.F. Weiser¹⁰², S.C. Wenzel³⁶, J.P. Wessels¹⁴², U. Westerhoff¹⁴², A.M. Whitehead¹²³, J. Wiechula⁶⁹, J. Wikne²³, G. Wilk⁸⁵, J. Wilkinson⁵³, G.A. Willems^{36,142}, M.C.S. Williams⁵³, E. Willsher¹⁰⁸, B. Windelband¹⁰², W.E. Witt¹²⁸, R. Xu⁷, S. Yalcin⁷⁸, K. Yamakawa⁴⁵, P. Yang⁷, S. Yano⁴⁵, Z. Yin⁷, H. Yokoyama^{131,79}, I.-K. Yoo²⁰, J.H. Yoon⁶⁰, V. Yurchenko³, V. Zaccolo⁵⁸, A. Zaman¹⁶, C. Zampolli³⁶, H.J.C. Zanoli¹¹⁹, N. Zardoshti¹⁰⁸, A. Zarochentsev¹³⁸, P. Závada⁶⁷, N. Zaviyalov¹⁰⁶, H. Zbroszczyk¹⁴⁰, M. Zhalov⁹⁶, H. Zhang⁷, X. Zhang⁷, Y. Zhang⁷, Z. Zhang^{132,7}, C. Zhao²³, N. Zhigareva⁶⁴, D. Zhou⁷, Y. Zhou⁸⁹, Z. Zhou²⁴, H. Zhu⁷, J. Zhu⁷, Y. Zhu⁷, A. Zichichi^{29,11}, M.B. Zimmermann³⁶, G. Zinovjev³, J. Zmeskal¹¹¹, S. Zou⁷,

Affiliation notes

ⁱ Deceased

ⁱⁱ Dipartimento DET del Politecnico di Torino, Turin, Italy

ⁱⁱⁱ M.V. Lomonosov Moscow State University, D.V. Skobeltsyn Institute of Nuclear Physics, Moscow, Russia

^{iv} Department of Applied Physics, Aligarh Muslim University, Aligarh, India

^v Institute of Theoretical Physics, University of Wrocław, Poland

Collaboration Institutes

¹ A.I. Alikhanyan National Science Laboratory (Yerevan Physics Institute) Foundation, Yerevan, Armenia

² Benemérita Universidad Autónoma de Puebla, Puebla, Mexico

³ Bogolyubov Institute for Theoretical Physics, National Academy of Sciences of Ukraine, Kiev, Ukraine

⁴ Bose Institute, Department of Physics and Centre for Astroparticle Physics and Space Science (CAPSS), Kolkata, India

⁵ Budker Institute for Nuclear Physics, Novosibirsk, Russia

⁶ California Polytechnic State University, San Luis Obispo, California, United States

- 7 Central China Normal University, Wuhan, China
- 8 Centre de Calcul de l'IN2P3, Villeurbanne, Lyon, France
- 9 Centro de Aplicaciones Tecnológicas y Desarrollo Nuclear (CEADEN), Havana, Cuba
- 10 Centro de Investigación y de Estudios Avanzados (CINVESTAV), Mexico City and Mérida, Mexico
- 11 Centro Fermi - Museo Storico della Fisica e Centro Studi e Ricerche "Enrico Fermi", Rome, Italy
- 12 Chicago State University, Chicago, Illinois, United States
- 13 China Institute of Atomic Energy, Beijing, China
- 14 Chonbuk National University, Jeonju, Republic of Korea
- 15 Comenius University Bratislava, Faculty of Mathematics, Physics and Informatics, Bratislava, Slovakia
- 16 COMSATS Institute of Information Technology (CIIT), Islamabad, Pakistan
- 17 Creighton University, Omaha, Nebraska, United States
- 18 Department of Physics, Aligarh Muslim University, Aligarh, India
- 19 Department of Physics, Ohio State University, Columbus, Ohio, United States
- 20 Department of Physics, Pusan National University, Pusan, Republic of Korea
- 21 Department of Physics, Sejong University, Seoul, Republic of Korea
- 22 Department of Physics, University of California, Berkeley, California, United States
- 23 Department of Physics, University of Oslo, Oslo, Norway
- 24 Department of Physics and Technology, University of Bergen, Bergen, Norway
- 25 Dipartimento di Fisica dell'Università 'La Sapienza' and Sezione INFN, Rome, Italy
- 26 Dipartimento di Fisica dell'Università and Sezione INFN, Cagliari, Italy
- 27 Dipartimento di Fisica dell'Università and Sezione INFN, Trieste, Italy
- 28 Dipartimento di Fisica dell'Università and Sezione INFN, Turin, Italy
- 29 Dipartimento di Fisica e Astronomia dell'Università and Sezione INFN, Bologna, Italy
- 30 Dipartimento di Fisica e Astronomia dell'Università and Sezione INFN, Catania, Italy
- 31 Dipartimento di Fisica e Astronomia dell'Università and Sezione INFN, Padova, Italy
- 32 Dipartimento di Fisica 'E.R. Caianiello' dell'Università and Gruppo Collegato INFN, Salerno, Italy
- 33 Dipartimento DISAT del Politecnico and Sezione INFN, Turin, Italy
- 34 Dipartimento di Scienze e Innovazione Tecnologica dell'Università del Piemonte Orientale and INFN Sezione di Torino, Alessandria, Italy
- 35 Dipartimento Interateneo di Fisica 'M. Merlin' and Sezione INFN, Bari, Italy
- 36 European Organization for Nuclear Research (CERN), Geneva, Switzerland
- 37 Faculty of Engineering and Science, Western Norway University of Applied Sciences, Bergen, Norway
- 38 Faculty of Nuclear Sciences and Physical Engineering, Czech Technical University in Prague, Prague, Czech Republic
- 39 Faculty of Science, P.J. Šafárik University, Košice, Slovakia
- 40 Frankfurt Institute for Advanced Studies, Johann Wolfgang Goethe-Universität Frankfurt, Frankfurt, Germany
- 41 Gangneung-Wonju National University, Gangneung, Republic of Korea
- 42 Gauhati University, Department of Physics, Guwahati, India
- 43 Helmholtz-Institut für Strahlen- und Kernphysik, Rheinische Friedrich-Wilhelms-Universität Bonn, Bonn, Germany
- 44 Helsinki Institute of Physics (HIP), Helsinki, Finland
- 45 Hiroshima University, Hiroshima, Japan
- 46 Hochschule Worms, Zentrum für Technologietransfer und Telekommunikation (ZTT), Worms, Germany
- 47 Horia Hulubei National Institute of Physics and Nuclear Engineering, Bucharest, Romania
- 48 Indian Institute of Technology Bombay (IIT), Mumbai, India
- 49 Indian Institute of Technology Indore, Indore, India
- 50 Indonesian Institute of Sciences, Jakarta, Indonesia
- 51 INFN, Laboratori Nazionali di Frascati, Frascati, Italy
- 52 INFN, Sezione di Bari, Bari, Italy
- 53 INFN, Sezione di Bologna, Bologna, Italy
- 54 INFN, Sezione di Cagliari, Cagliari, Italy
- 55 INFN, Sezione di Catania, Catania, Italy
- 56 INFN, Sezione di Padova, Padova, Italy
- 57 INFN, Sezione di Roma, Rome, Italy
- 58 INFN, Sezione di Torino, Turin, Italy

- 59 INFN, Sezione di Trieste, Trieste, Italy
- 60 Inha University, Incheon, Republic of Korea
- 61 Institut de Physique Nucléaire d'Orsay (IPNO), Institut National de Physique Nucléaire et de Physique des Particules (IN2P3/CNRS), Université de Paris-Sud, Université Paris-Saclay, Orsay, France
- 62 Institute for Nuclear Research, Academy of Sciences, Moscow, Russia
- 63 Institute for Subatomic Physics, Utrecht University/Nikhef, Utrecht, Netherlands
- 64 Institute for Theoretical and Experimental Physics, Moscow, Russia
- 65 Institute of Experimental Physics, Slovak Academy of Sciences, Košice, Slovakia
- 66 Institute of Physics, Bhubaneswar, India
- 67 Institute of Physics of the Czech Academy of Sciences, Prague, Czech Republic
- 68 Institute of Space Science (ISS), Bucharest, Romania
- 69 Institut für Kernphysik, Johann Wolfgang Goethe-Universität Frankfurt, Frankfurt, Germany
- 70 Instituto de Ciencias Nucleares, Universidad Nacional Autónoma de México, Mexico City, Mexico
- 71 Instituto de Física, Universidade Federal do Rio Grande do Sul (UFRGS), Porto Alegre, Brazil
- 72 Instituto de Física, Universidad Nacional Autónoma de México, Mexico City, Mexico
- 73 iThemba LABS, National Research Foundation, Somerset West, South Africa
- 74 Johann-Wolfgang-Goethe Universität Frankfurt Institut für Informatik, Fachbereich Informatik und Mathematik, Frankfurt, Germany
- 75 Joint Institute for Nuclear Research (JINR), Dubna, Russia
- 76 Konkuk University, Seoul, Republic of Korea
- 77 Korea Institute of Science and Technology Information, Daejeon, Republic of Korea
- 78 KTO Karatay University, Konya, Turkey
- 79 Laboratoire de Physique Subatomique et de Cosmologie, Université Grenoble-Alpes, CNRS-IN2P3, Grenoble, France
- 80 Lawrence Berkeley National Laboratory, Berkeley, California, United States
- 81 Lund University Department of Physics, Division of Particle Physics, Lund, Sweden
- 82 Nagasaki Institute of Applied Science, Nagasaki, Japan
- 83 Nara Women's University (NWU), Nara, Japan
- 84 National and Kapodistrian University of Athens, School of Science, Department of Physics, Athens, Greece
- 85 National Centre for Nuclear Research, Warsaw, Poland
- 86 National Institute of Science Education and Research, HBNI, Jatni, India
- 87 National Nuclear Research Center, Baku, Azerbaijan
- 88 National Research Centre Kurchatov Institute, Moscow, Russia
- 89 Niels Bohr Institute, University of Copenhagen, Copenhagen, Denmark
- 90 Nikhef, National institute for subatomic physics, Amsterdam, Netherlands
- 91 NRC Kurchatov Institute IHEP, Protvino, Russia
- 92 NRNU Moscow Engineering Physics Institute, Moscow, Russia
- 93 Nuclear Physics Group, STFC Daresbury Laboratory, Daresbury, United Kingdom
- 94 Nuclear Physics Institute of the Czech Academy of Sciences, Řež u Prahy, Czech Republic
- 95 Oak Ridge National Laboratory, Oak Ridge, Tennessee, United States
- 96 Petersburg Nuclear Physics Institute, Gatchina, Russia
- 97 Physics department, Faculty of science, University of Zagreb, Zagreb, Croatia
- 98 Physics Department, Panjab University, Chandigarh, India
- 99 Physics Department, University of Jammu, Jammu, India
- 100 Physics Department, University of Rajasthan, Jaipur, India
- 101 Physikalisches Institut, Eberhard-Karls-Universität Tübingen, Tübingen, Germany
- 102 Physikalisches Institut, Ruprecht-Karls-Universität Heidelberg, Heidelberg, Germany
- 103 Physik Department, Technische Universität München, Munich, Germany
- 104 Research Division and ExtreMe Matter Institute EMMI, GSI Helmholtzzentrum für Schwerionenforschung GmbH, Darmstadt, Germany
- 105 Rudjer Bošković Institute, Zagreb, Croatia
- 106 Russian Federal Nuclear Center (VNIIEF), Sarov, Russia
- 107 Saha Institute of Nuclear Physics, Kolkata, India
- 108 School of Physics and Astronomy, University of Birmingham, Birmingham, United Kingdom
- 109 Sección Física, Departamento de Ciencias, Pontificia Universidad Católica del Perú, Lima, Peru

- 110 Shanghai Institute of Applied Physics, Shanghai, China
- 111 Stefan Meyer Institut für Subatomare Physik (SMI), Vienna, Austria
- 112 SUBATECH, IMT Atlantique, Université de Nantes, CNRS-IN2P3, Nantes, France
- 113 Suranaree University of Technology, Nakhon Ratchasima, Thailand
- 114 Technical University of Košice, Košice, Slovakia
- 115 Technische Universität München, Excellence Cluster 'Universe', Munich, Germany
- 116 The Henryk Niewodniczanski Institute of Nuclear Physics, Polish Academy of Sciences, Cracow, Poland
- 117 The University of Texas at Austin, Austin, Texas, United States
- 118 Universidad Autónoma de Sinaloa, Culiacán, Mexico
- 119 Universidade de São Paulo (USP), São Paulo, Brazil
- 120 Universidade Estadual de Campinas (UNICAMP), Campinas, Brazil
- 121 Universidade Federal do ABC, Santo Andre, Brazil
- 122 University College of Southeast Norway, Tonsberg, Norway
- 123 University of Cape Town, Cape Town, South Africa
- 124 University of Houston, Houston, Texas, United States
- 125 University of Jyväskylä, Jyväskylä, Finland
- 126 University of Liverpool, Liverpool, United Kingdom
- 127 University of Split, Faculty of Electrical Engineering, Mechanical Engineering and Naval Architecture, Split, Croatia
- 128 University of Tennessee, Knoxville, Tennessee, United States
- 129 University of the Witwatersrand, Johannesburg, South Africa
- 130 University of Tokyo, Tokyo, Japan
- 131 University of Tsukuba, Tsukuba, Japan
- 132 Université Clermont Auvergne, CNRS/IN2P3, LPC, Clermont-Ferrand, France
- 133 Université de Lyon, Université Lyon 1, CNRS/IN2P3, IPN-Lyon, Villeurbanne, Lyon, France
- 134 Université de Strasbourg, CNRS, IPHC UMR 7178, F-67000 Strasbourg, France, Strasbourg, France
- 135 Université Paris-Saclay Centre d'Études de Saclay (CEA), IRFU, Department de Physique Nucléaire (DPhN), Saclay, France
- 136 Università degli Studi di Pavia, Pavia, Italy
- 137 Università di Brescia, Brescia, Italy
- 138 V. Fock Institute for Physics, St. Petersburg State University, St. Petersburg, Russia
- 139 Variable Energy Cyclotron Centre, Kolkata, India
- 140 Warsaw University of Technology, Warsaw, Poland
- 141 Wayne State University, Detroit, Michigan, United States
- 142 Westfälische Wilhelms-Universität Münster, Institut für Kernphysik, Münster, Germany
- 143 Wigner Research Centre for Physics, Hungarian Academy of Sciences, Budapest, Hungary
- 144 Yale University, New Haven, Connecticut, United States
- 145 Yonsei University, Seoul, Republic of Korea